

MASARYKOVA UNIVERZITA
PŘÍRODOVĚDECKÁ FAKULTA
ÚSTAV TEORETICKÉ FYZIKY A ASTROFYZIKY

Bakalářská práce

BRNO 2012

JURAJ ČURPEK



MASARYKOVA UNIVERZITA
PŘÍRODOVĚDECKÁ FAKULTA
ÚSTAV TEORETICKÉ FYZIKY A ASTROFYZIKY



Analýza mikrovlnného kosmologického pozadí

Bakalářská práce

Juraj Čurpek

Vedoucí práce: Mgr. Filip Hroch, Ph.D. Brno 2012

Bibliografický záznam

Autor: Juraj Čurpek
Přírodovědecká fakulta, Masarykova univerzita
Ústav teoretické fyziky a astrofyziky

Název práce: Analýza mikrovlnného kosmologického pozadí

Studijní program: Aplikovaná fyzika

Studijní obor: Astrofyzika

Vedoucí práce: Mgr. Filip Hroch, Ph.D.

Akademický rok: 2011/2012

Počet stran: ix + 45

Klíčová slova: záření; velký třesk; anizotropie; WMAP; power spektrum; křivost

Bibliographic Entry

Author: Juraj Čurpek
Faculty of Science, Masaryk University
Department of Theoretical Physics and Astrophysics.

Title of Thesis: On Analysis Of Cosmic Microwave Background

Degree Programme: Applied physics

Field of Study: Astrophysics

Supervisor: Mgr. Filip Hroch, Ph.D.

Academic Year: 2011/2012

Number of Pages: ix + 45

Keywords: radiation; Big Bang; anisotropies; WMAP; power spectrum; curvature

Abstrakt

V této bakalářské práci se věnujeme studiu mikrovlnného kosmologického pozadí za použití dat pořízených družicí WMAP. Zejména nás zajímají fluktuace teploty, které jsou uloženy v mapách zachycujících celou oblohu v mikrovlnné části spektra. Naší snahou je výpočet power spektra, které popisuje tyto fluktuace, a následné srovnání s výsledky vědeckého týmu WMAP.

Abstract

In this thesis we study the cosmic microwave background radiation from data obtained by the Wilkinson Microwave Anisotropy Probe (WMAP). Especially, the topic of our interest are its temperature fluctuations which are encoded in full-sky maps. We are eager to determine the angular power spectrum which is describing the temperature anisotropies of the cosmic microwave background radiation and compare it with the results from WMAP science team.



Masarykova univerzita

Přírodovědecká fakulta



ZADÁNÍ BAKALÁŘSKÉ PRÁCE

Student : Juraj Čurpek
Studijní program : Aplikovaná fyzika
Studijní obor : Astrofyzika

Ředitel Ústavu teoretické fyziky a astrofyziky PŘF MU Vám ve smyslu Studijního a zkušebního řádu MU určuje bakalářskou práci s tématem:

Analyza mikrovlnného kosmologického pozadí

On Analysis Of Cosmic Microwave Background

Práce bude napsána v jazyce anglickém.

Zásady pro vypracování:

Mikrovlnné kosmologické záření je sledováno již asi půl století z povrchu zemského, avšak teprve vypuštění kosmických družic, zaměřených na jeho detekci, prosté šumu známého z pozemských stanic, zaznamenalo průlom v pochopení a detailní analýze kosmologického pozadí. Cílem této práce je analýza pozorování kosmického záření. Ke úspěšnému zvládnutí práce je třeba běžná rutina v použití základních metod zpracování dat z družic, matematické statistiky a příslušných fyzikálních oblastí.

Vedoucí bakalářské práce : Mgr. Filip Hroch, Ph.D.
Datum zadání bakalářské práce : září 2011
Datum odevzdání bakalářské práce : dle harmonogramu ak. roku 2011/2012

V Brně dne 7. 12. 2011


Prof. Rikard von Unge, Ph.D.
ředitel Ústavu teoretické fyziky a astrofyziky
PřF MU

Zadání bakalářské práce převzal dne: 14. 12. 2011

Podpis studenta



Poděkování

Na tomto místě bych chtěl poděkovat vedoucímu mé bakalářské práce, Filipu Hrochovi, za jeho neocenitelné odborné rady a náměty, které mě inspirovaly při jejím psaní.

Prohlášení

Prohlašuji, že jsem svoji bakalářskou práci vypracoval samostatně s využitím informačních zdrojů, které jsou v práci citovány.

Brno 18. května 2012

.....
Juraj Čurpek

Contents

Chapter 1. Cosmic Microwave Background Radiation	1
1.1 Spectrum of the CMB	2
1.2 Origin of the CMB	3
1.2.1 Big Bang and CMB	3
1.3 CMB temperature anisotropies	6
1.3.1 Acoustic oscillations	8
1.3.2 Dipole anisotropy	9
1.3.3 Foreground contamination	11
1.4 Discovery and the history of the measurements of the CMB	12
1.4.1 Discovery of the CMB	12
1.4.2 Timeline of the CMB measurements	13
Chapter 2. A brief introduction to cosmology	14
2.1 Foundations	14
2.2 Geometry of the universe	14
2.3 Expansion	16
Chapter 3. WMAP	20
3.1 WMAP mission	20
3.1.1 Mission timeline	20
3.1.2 Technical specification	21
3.1.3 Observations	22
3.2 Data products and software	24
3.2.1 Sky maps	24
3.2.2 Foreground exclusion masks	25
3.2.3 Beam transfer functions	26
3.2.4 HEALPix	27
Chapter 4. Analysis of CMB angular power spectrum	28
4.1 Angular power spectrum	28
4.1.1 Estimation	28
4.1.2 Bias of the CMB power spectrum estimation	28
4.2 Interpretation of acoustic peaks	30

Chapter 5. Results	33
5.1 From sky maps to power spectra	33
5.2 Fitting	39
List of References	42

Introduction

If we, the humans, look at the sky during the cloudless night, we can see many shining stars, several planets and our Moon situated in a vast, dark universe. However, the hypothetical observers capable of microwave vision (probably aliens) would see the entire universe filled with the faint "light" coming from all directions, which is called by the humans the cosmic microwave background radiation (CMB).

Because the humans can not perceive any radiation in the microwave part of the electromagnetic spectrum, CMB was discovered in the 20th century when the astronomers had an instrument which could detect the microwave radiation from space. Furthermore, a detection of this weak radiation was not a piece of cake. But finally, in 1965 two radioastronomers Arno Penzias and Robert Wilson accidentally detected a feeble radiation with unknown origin, coming to us from all directions in the sky, with the effective temperature about 3 K. At first, they thought that it is just some systematic noise, but soon realized that this radiation had been predicted in 1948 by George Gamow, Ralph Alpher, and Robert Herman as a relic of the evolution of the early universe.[1]

From its discovery there have been many experiments observing CMB with better resolution and sensitivity, which lead to the discovery of the temperature fluctuations of CMB. In this bachelor thesis we analyse these very tiny temperature anisotropies from the maps which were created on the basis of observations from The Wilkinson Microwave Anisotropy Probe (WMAP). Our goal is to determine the most important physical quantity – the angular power spectrum, which yields a lot of information about the nature of the universe. In addition, the CMB anisotropies are so important for the scientific world, that in 2006 John Mather and George Smoot have been awarded the Nobel Prize because they discovered the temperature anisotropies of CMB using COBE satellite.[2]

This thesis consists of five chapters. The first chapter is about CMB and its main features. In the second one is a short description of the Big Bang model. In the third chapter the WMAP spacecraft and the data description which we used for our analysis are presented. The fourth chapter contains information about how we analysed the CMB power spectrum and in the fifth chapter are presented our results.

Chapter 1

Cosmic Microwave Background Radiation

In our universe there is a low-intensity radiation with an equivalent temperature about 2.73 K which comes from all directions and is detectable in the microwave part of the electromagnetic spectrum. This almost isotropic radiation is formally called the cosmic microwave background radiation or relic radiation, because it is the memento from the time when the universe was about 380 000 years old. CMB is not perfectly isotropic due to little anisotropies, and as we will see, they can provide us a lot of information about the universe we live in.[3]

This chapter deals with the cosmic microwave background radiation, especially with its spectrum, origin, anisotropies which we will analyse in the next chapters. In addition, there are also sections about its accidental discovery and a short chronological list of main CMB experiments.

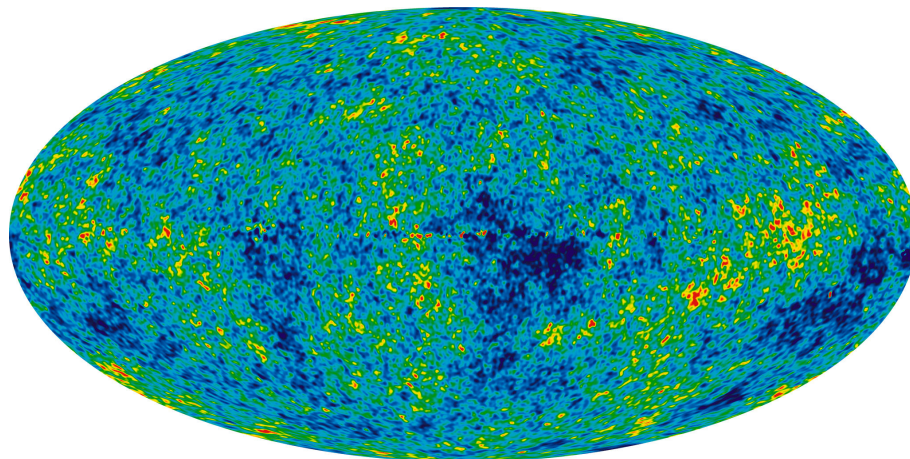


Figure 1.1: The CMB temperature anisotropy full-sky map taken by WMAP. (NASA / WMAP Science Team)

1.1 Spectrum of the CMB

CMB, which is prevalent radiation field in the universe, has a form of the black body thermal radiation which is almost isotropic. In 1991, FIRAS¹ instrument of COBE² measured the spectrum of CMB and confirmed that it has the perfect black body spectrum which almost fits the theoretical prediction of black body with the temperature of $T_0 = (2.725 \pm 0.002)$ K (Figure 1.2).[4]

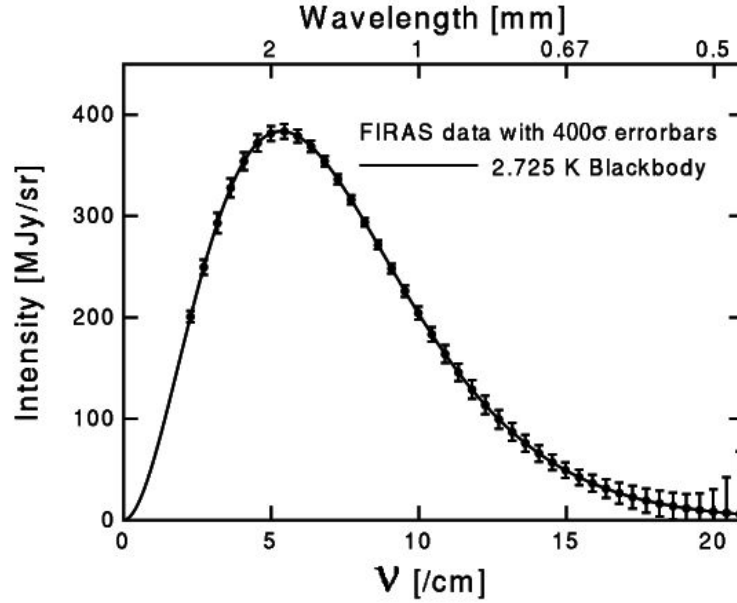


Figure 1.2: CMB spectrum measured by COBE. (NASA / COBE / FIRAS)

Due to the nature of the CMB as the almost perfect black body, the specific intensity I_ν of the CMB radiation is very close to:

$$I_\nu = \frac{2h\nu^3}{c^2} \frac{1}{(e^{h\nu/k_B T_0} - 1)}, \quad (1.1)$$

where h is a Planck's constant, c is the speed of light in vacuum, ν is the frequency and k_B is the Boltzmann constant. After calculation it corresponds to a peak intensity $I_{\max} \sim 3.7 \times 10^{-18} \text{ W m}^{-2} \text{ Hz}^{-1} \text{ sr}^{-1}$ at $\nu_{\max} \sim 160 \text{ GHz}$, an energy density $u_\gamma \sim 4 \times 10^{-14} \text{ J m}^{-3}$, and the photon density $n_\gamma \sim 4 \times 10^8 \text{ photons m}^{-3}$. [5]

It is obvious that the present CMB temperature of $T_0 = 2.725 \text{ K}$ is insufficient to ionize hydrogen, but during the recombination era the temperature was about 3000 K. This decrease in temperature is caused by a cosmological redshift as a result of the fact that the universe has been expanding since the Big Bang. The cosmological redshift can be described by following equation:

¹FIRAS is an acronym for Far InfraRed Absolute Spectrometer.

²COBE is an acronym for Cosmic Background Explorer.

$$1 + z = \frac{\lambda_{\text{now}}}{\lambda_{\text{then}}} = \frac{R_{\text{now}}}{R_{\text{then}}}, \quad (1.2)$$

where z is the redshift and R is the time-dependent cosmic scale factor for different time. As we can see, the wavelengths of the CMB increase by the same factor as the universe expands.[6]

Furthermore, according to the Wien's displacement law the peak wavelength is indirectly proportional to the black body temperature:

$$\lambda = \frac{2.897 \times 10^{-3} \text{ m K}}{T}. \quad (1.3)$$

By combining the equations (1.2) and (1.3) we get a new equation which describes the relation between the expansion of the universe and the CMB temperature:

$$\frac{T_{\text{then}}}{T_{\text{now}}} = \frac{R_{\text{now}}}{R_{\text{then}}}. \quad (1.4)$$

The observed decrease in CMB temperature is $T_{\text{then}}/T_{\text{now}} = 3000 \text{ K}/2.73 \text{ K} \approx 1100$, which means that the universe has expanded by a factor of 1100 since the moment when CMB was created.

1.2 Origin of the CMB

The Big Bang theory predicts the existence of the cosmic microwave background radiation. Since its discovery in 1965, it has been considered as the most conclusive evidence for the Big Bang. According to the WMAP 7-year results one occurred 13.75 ± 0.13 billion years ago, which is de facto the age of the universe.[7]

1.2.1 Big Bang and CMB

In the Big Bang models, scientists assume that our universe began about 13.75 billion years ago as the infinitesimally small point containing all the matter and the energy of the universe which was immensely hot and dense. Technically, at a very beginning of the universe, its density was above the so-called Planck density which is roughly $10^{96} \text{ kg m}^{-3}$ and there is no physical theory capable of describing the universe at this time. The general relativity can be used since the moment when the age of the universe was equal to the Planck time, which is approximately 10^{-43} s . At that time the universe density dropped to the Planck density, its size was about 10^{-35} m and the temperature was about 10^{32} K .

Then the universe had been cooling and expanding until a cosmic inflation occurred, which is a short period of exponential expansion happened about $10^{-35} - 10^{-32}$ seconds after the Big Bang. It caused the rapid increase in a linear size of the early universe by a factor of 10^{26} . Since the inflation the universe has been expanding in significantly slower rate than during the inflation period.

Approximately hundred seconds after the Big Bang, the universe cooled to the temperature about 10^9 K when the protons and neutrons formed atomic nuclei and the lightest chemical elements were created. The result of this nucleosynthesis was that about

three-quarters of the mass of the universe were in a form of the hydrogen and approximately one-quarter in a form of the helium with a trace abundance of lithium.

The baryons and the photons were in the form of a hot plasma, sometimes called primordial, until the universe cooled to the temperature at which the electrons and the protons could combine and form neutral hydrogen atoms. Since that moment when the matter and the radiation decoupled, the universe became transparent to the light. This occurred about 380 000 years ago when the temperature of the universe was about 3000 K and this era is called the recombination epoch. The radiation released during this era has been traveled almost undisturbed until the present day. Due to the cosmological redshift, its present temperature is $T_0 = 2.725$ K and the peak is in the microwave region of the spectrum.

The recombination epoch occurred at a cosmological redshift of 1100 which means that the universe was 1100-times smaller than in present day. Although the ionization energy of a hydrogen atom is 13.6 eV, the recombination occurred when the universe had cooled to a temperature equivalent to the characteristic energy³ of 0.3 eV. This delay was mainly due to the large entropy of the universe. It caused that the electron recombination rate was slightly higher than the photodissociation rate. In addition, each recombined electron emitted photon with an energy 13.6 eV which was capable of ionizing another neutral atom.[8][9]

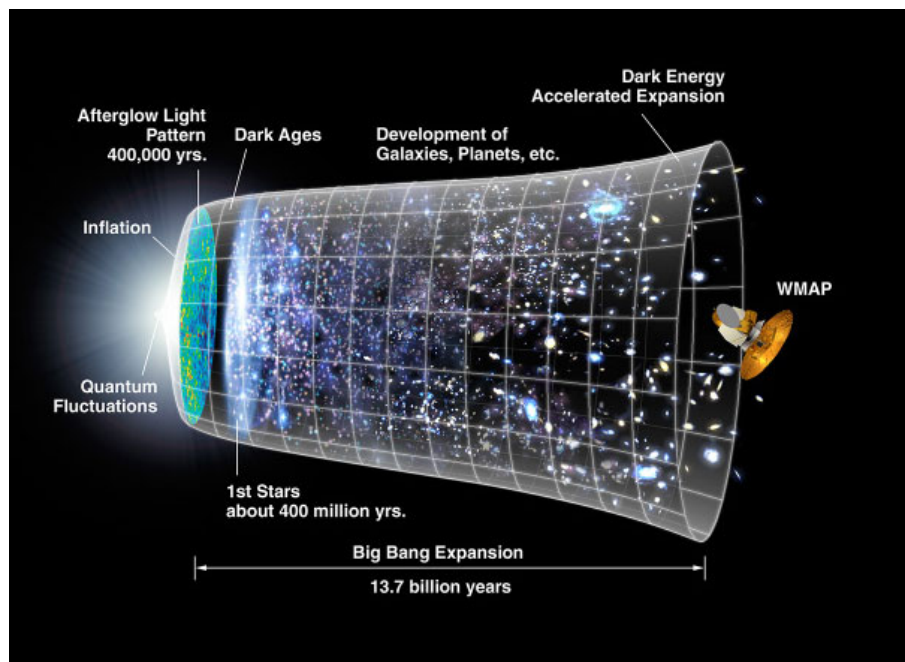


Figure 1.3: CMB timeline. (NASA / WMAP Science Team)

³The characteristic energy is the mean energy associated with a particle in thermal equilibrium at temperature T and it is equal to $k_B T$, where k_B is the Boltzmann constant.[10]

The surface of last scattering

The CMB we observe today comes from the surface of last scattering of the universe (Figure 1.4). It is defined as a surface around the observer where the radius of the shell is the distance each photon has traveled since it was last scattered at the recombination epoch. It is impossible to observe what happened beyond this surface due to the rapid scattering the photons off the electrons. On the other hand, closer than this surface the universe is essentially transparent. That is why the CMB is the oldest radiation possibly observed in the universe.[11]

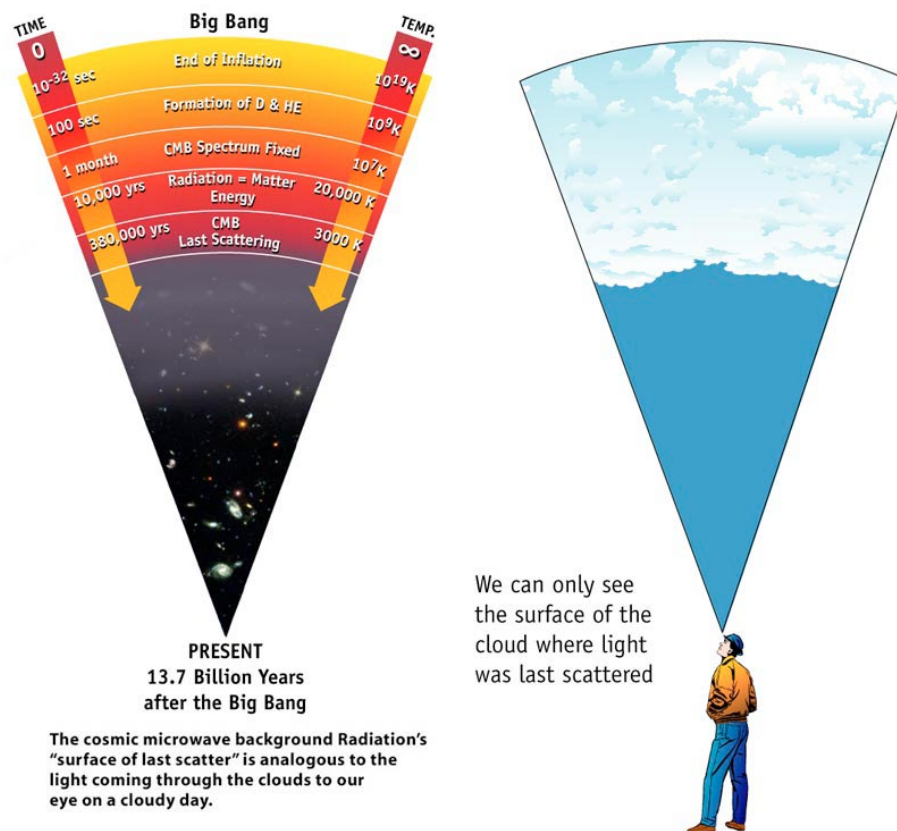


Figure 1.4: The surface of last scattering. (NASA / WMAP Science Team)

1.3 CMB temperature anisotropies

When we look at the full-sky temperature map (Figure 1.5) of the CMB radiation, we can see a very little spots which have size about 1° degree or less in diameter and their temperature is slightly different from the average value T_0 . They represent temperature anisotropies which relative value is $\delta T \approx 10^{-5}$. To specify the statistical properties of the anisotropy map, if the anisotropies have the Gaussian distribution, we use either the angular correlation function $C(\theta)$ or the angular power spectrum C_l which is a Legendre transform⁴ of $C(\theta)$.

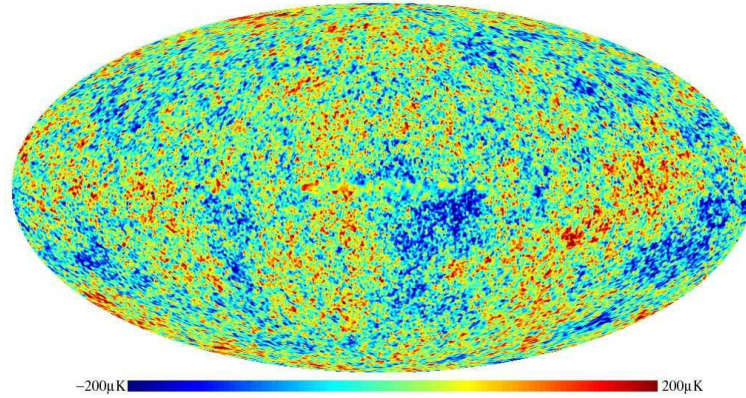


Figure 1.5: WMAP anisotropy map. (NASA / WMAP Science Team)

The angular correlation function is defined as the value of the product of temperatures at two points on celestial sphere separated by an angle θ [13]:

$$C(\theta) = \langle \Delta T(l, b) \Delta T(l', b') \rangle. \quad (1.5)$$

We can also make a harmonic analysis of the CMB anisotropy map. Then we expand the temperature fluctuations $\Delta T(l, b) = T(l, b) - T_0$ in the direction of an angular position (l, b) into spherical harmonics, which is analogous to the Fourier transform:

$$\Delta T(l, b) = \sum_{l=1}^{\infty} \sum_{m=-l}^l a_{lm} Y_{lm}(l, b), \quad (1.6)$$

where $Y_{lm}(l, b)$ are complex spherical harmonic functions and a_{lm} are also complex expansion coefficients. Using these coefficients of expansion we define the angular power spectrum as their ensemble average:

$$C_l = \langle |a_{lm}|^2 \rangle. \quad (1.7)$$

If we average the expansion coefficients a_{lm} over $(2l + 1)$ values of m , we get :

$$C_l = \frac{1}{2l + 1} \sum_{m=-l}^l |a_{lm}|^2 = \frac{1}{2l + 1} \sum_{m=-l}^l a_{lm}^i a_{lm}^{j*}. \quad (1.8)$$

⁴A transformation widely used in physics when one function of several variables is transformed into the new function which depends on partial derivatives of the original function with respect to some of the original independent variables.[12]

The angular power spectrum comprises either positive and negative temperature fluctuations (in summation are all terms ≥ 0). Furthermore, we see at the Figure 1.6 that the angular power spectrum is plotted as $l(l+1)C_l/2\pi$.^[14]

Because we used for the estimation of the angular power spectra the average of $(2l+1)$ squares of a_{lm} coefficients, there is unavoidable error called the cosmic variance ^[48]:

$$\delta C_l = \sqrt{\frac{2}{2l+1}}. \quad (1.9)$$

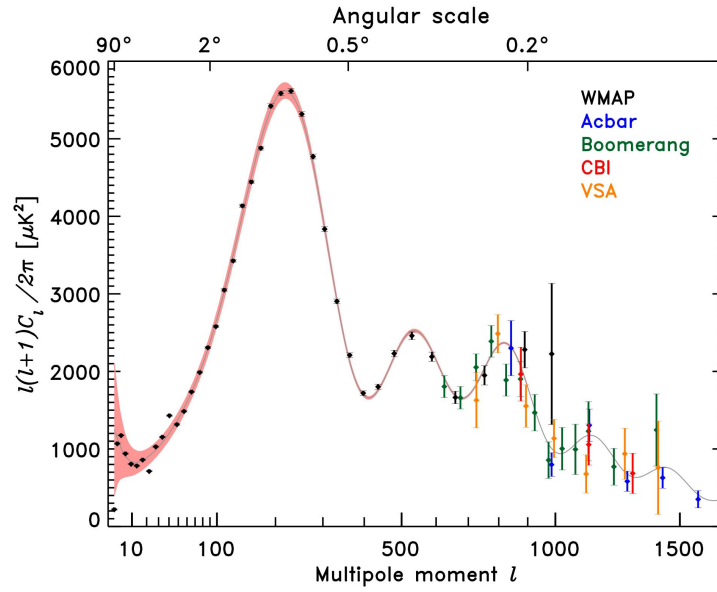


Figure 1.6: Angular power spectrum. (NASA / WMAP Science Team)

The relation between the angular correlation function and the angular power spectrum is ^[13]:

$$C(\theta) = \frac{1}{4\pi} \sum_l (2l+1) C_l P_l(\cos\theta), \quad (1.10)$$

where P_l is the Legendre polynomial⁵ of order l . The spherical harmonic order and angular scale are related as $\theta \sim 180^\circ/l$.

In addition, because the Legendre polynomials are orthogonal⁶, we can get the another equation describing the relation which describes the between the angular correlation function and the angular power spectrum ^[17] :

$$C_l = 2\pi \int_0^\pi C(\theta) P_l(\cos\theta) \sin\theta d\theta. \quad (1.11)$$

⁵Legendre polynomials are solutions to the Legendre equation.^[15]

⁶Orthogonality in this case means that for $m \neq n$ an integral $\int_{-1}^1 P_m(x)P_n(x)dx = 0$.^[16]

In general, there are two kinds of the CMB anisotropies: primary and secondary.

The primary anisotropies have their origin at the surface of last scattering. They are the result of a density perturbations in the early universe which were crucial for the galaxies and clusters of galaxies formation.

The secondary anisotropies affected the CMB by processes which occurred between the surface of the last scattering and the observer.[18]

In this thesis we describe only the main reasons for the CMB temperature anisotropies which are:

- Acoustic oscillations which caused the characteristic acoustic peaks
- Dipole anisotropy which is caused by the Doppler effect

If we want to perform an analysis of CMB anisotropies, at first, we have to subtract the foreground emission (Subsection 1.3.3) and dipole anisotropy (Subsection 1.3.2). Then the remaining radiation is almost isotropic with tiny temperature fluctuations and looks like at Figure 1.5.

1.3.1 Acoustic oscillations

Due to the quantum mechanical density fluctuations shortly after Big Bang, there were randomly underdense and overdense regions – density perturbations of space. These regions rapidly expanded due to inflation that they exceeded the particle horizon⁷ and were not casually connected. However, after some time, when universe expanded enough they entered the particle horizon and were able to react with the surrounding. The density perturbations entered the particle horizon according to their size. The smaller ones, entered it earlier than the perturbations of larger size. So, there were also perturbations which entered the horizon after recombination and did not participate in oscillations. On the other hand, the smaller perturbations which correspond to the acoustic waves with the very small wavelength were dumped due to the photon diffusion.

Due to the gravity the overdense regions were compressed, and consequently became hotter. The collapse of these regions continued until radiation pressure surpassed the gravity and caused the expansion (rarefaction) of these regions and thereby their cooling (Figure 1.7). This created acoustic waves traversing the universe, so these waves consisting of the photon-baryon fluid executed simple harmonic motion.[14][19]

The sound velocity of the acoustic waves before recombination was:

$$v_s = \sqrt{\frac{\partial p}{\partial \rho}} = \frac{c}{\sqrt{3}}, \quad (1.12)$$

where c is the speed of light in the vacuum.

The acoustic waves vanished at recombination, because the photons decoupled and have been propagating through the universe carrying the imprints of the hotter (overdense) and cooler (underdense) regions which we see as the temperature anisotropies (Figure 1.5).

⁷The spatial boundary that represents the farthest point that can be observed at specific time. As the universe expands, the particle horizon changes with time according to the rate of the expansion.[14]

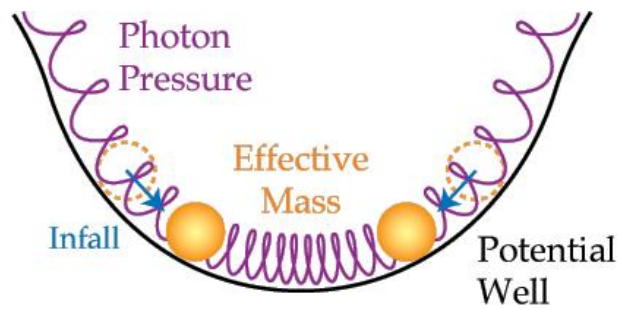


Figure 1.7: Analogy of gravity and the photon pressure to the balls and string. (Wayne Hu: A Tour of CMB Physics web page)

Furthermore, when the photons started to travel freely from the regions of various density at last scattering surface, their frequency was affected by the so-called Sachs-Wolfe effect. If the photons traveled from the overdense regions, they climbed out of the potential well of the density fluctuation, which redshifted them due to the gravity, so their frequency slightly decreased. On the other hand, if they traveled from the underdense regions, they were blueshifted, so their frequency slightly increased.[14]

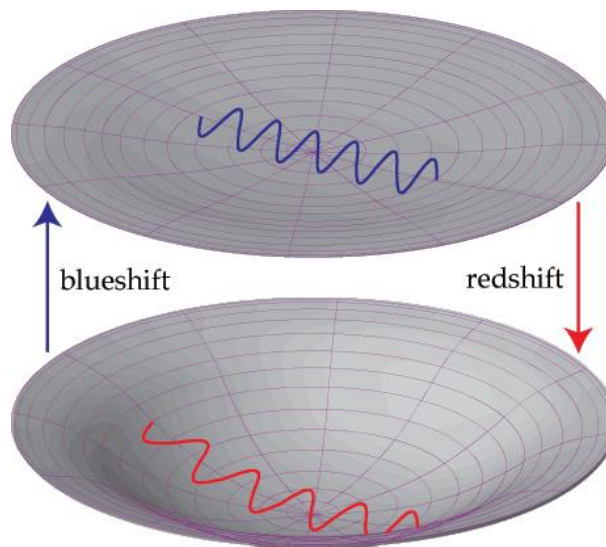


Figure 1.8: Sachs-Wolfe effect. (Wayne Hu: A Tour of CMB Physics web page)

The acoustic oscillations are responsible for the fact that there are peaks and troughs in the angular power spectra (Figure 1.6). Their deeper description and interpretation is in Section 4.2.

1.3.2 Dipole anisotropy

The Earth is not at the rest. It moves around the Sun. The Sun orbits the centre of the Milky Way Galaxy. The Milky Way Galaxy orbits in the Local Group of Galaxies. The

Local Group falls toward the Virgo Cluster of Galaxies. It also moves with respect to the cosmic microwave background (has a so-called peculiar velocity relative to the CMB comoving frame), so there is a Doppler shift of the CMB. This shift in the wavelength changes the temperature of CMB T_0 to T' measured by the moving observer:

$$T' = \frac{T_0 \sqrt{1 - v^2/c^2}}{1 - (v/c) \cos \theta}, \quad (1.13)$$

where T' also depends on the angle between the direction of motion and direction of observation θ . If the peculiar velocity is much smaller than the speed of light, we can approximate the equation (1.13) as:

$$T' \simeq T_0 \left(1 + \frac{v}{c} \cos \theta \right) = T_0 + T_0 \left(\frac{v}{c} \cos \theta \right), \quad (1.14)$$

where the term $T_0 (v/c \cdot \cos \theta)$ is called the dipole anisotropy.[14]

The CMB is blueshifted to a higher effective temperature in the direction of the Earth's motion ($\theta = 0$) and red shifted to a lower effective temperature in the direction opposite the Earth's motion ($\theta = \pi$) (Figure 1.9).

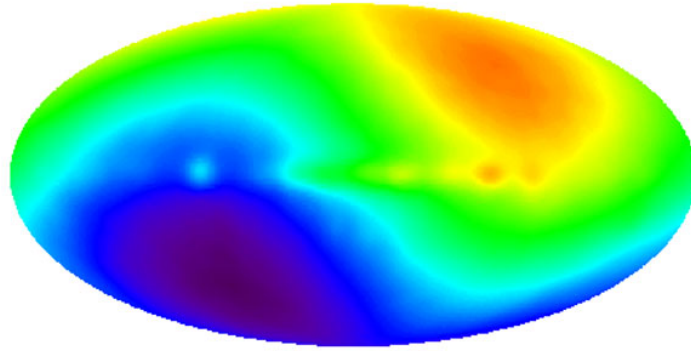


Figure 1.9: Dipole measured by COBE. (NASA / COBE / DMR)

The measurements of the amount of the dipole anisotropy using COBE DMR showed that there is the dipole anisotropy about 3 mK in the direction of the constellation Leo. By using these measurements it is possible to determine the velocity of the Sun with the respect to the comoving frame of CMB, which is $v = (369.0 \pm 2.5)$ km/s towards $(l, b) = (263.85^\circ \pm 0.10^\circ, 48.25^\circ \pm 0.04^\circ)$.

Furthermore, the Solar System velocity implies a velocity for the Galaxy and the Local Group of galaxies relative to the CMB. The velocity of the Local Group with the respect to the comoving frame of CMB is $v = (627 \pm 22)$ km/s in a direction $(l, b) = (276^\circ \pm 3^\circ, 30^\circ \pm 3^\circ)$. [20]

1.3.3 Foreground contamination

The CMB is contaminated by the Galactic and extragalactic emission which have different properties. Thus the observations of the CMB anisotropy must be distinguished from foreground emission. The diffuse Galactic radio emission, which significantly alters CMB, has three primary mechanisms:

- Synchrotron radiation – emitted by an interaction of relativistic electrons with the magnetic field of our Galaxy
- Dust grains emission – caused by the excitation of the vibrational modes and has a modified black body spectrum
- Free-free radiation – produced by the scattering of less energetic electrons from each other and ionized nuclei

While the CMB has a blackbody spectrum at a given temperature, Galactic and extragalactic contributions have a different spectral dependence. For instance, at the temperature of 2.73 K the peak of the CMB intensity lies at about 160 GHz, dust and dusty external galaxies are expected to dominate the CMB at higher frequencies from about 300 GHz, whereas synchrotron and free-free emission dominate at lower frequencies. Observed synchrotron emission dominates at 20–40 GHz and free-free emission is dominant at 30–60 GHz. [21] [22]

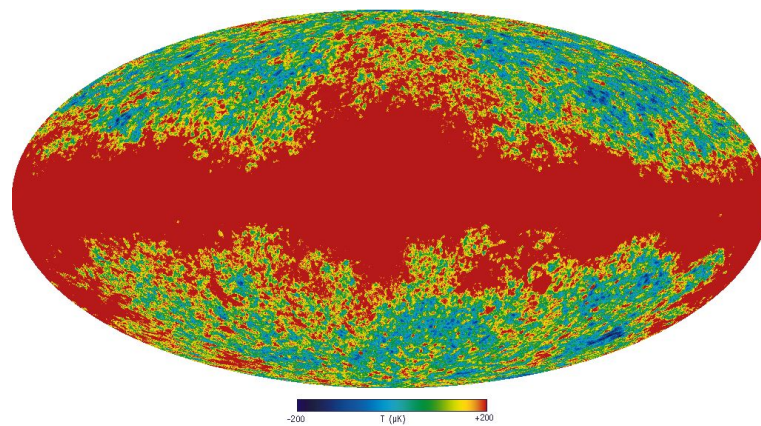


Figure 1.10: Full-sky map of the CMB anisotropy and foreground signal from our Galaxy in K band. (NASA / WMAP Science Team)

1.4 Discovery and the history of the measurements of the CMB

1.4.1 Discovery of the CMB

In 1960, Bell Laboratories built horn-shaped antenna in Holmdel, New Jersey to use it for radio transmission accros long distances using a balloon satellite system called Echo. However, after several years this system appeared to be obsolete and because it was not used for commercial purposes, it became an instrument for astrophysical research.



Figure 1.11: Horn antenna of great discovery. (Photo Credit: Bell Laboratories)

Two scientists, Arno Penzias and Robert Wilson started to use this antenna to study a radio emission from our Galaxy. However, they soon discovered that their measurements were contaminated by an unidentified noise. They were trying to eliminate it by identifying the source, but after exclusion of the Sun, planets or any celestial source the can identify and man-made sources like radar or radio broadcasting, they were so desperate, that they even accused the pigeons for this noise.

Fortunately, Arno Penzias came across an article by Princeton University physicist Robert Dicke who had predicted that if the Big Bang really ocured, there would be the cosmic microwave radiation – weak radiation throughout the universe and after that he realized that the noise is actually the CMB. They got together to share their results and published them in the *Astrophysical Journal* as an article "A measurement of excess antenna temperature at 4080 Mc/s"[23] from May 13, 1965. In 1978, Penzias and Wilson were awarded the Nobel Prize in Physics for their discovery.[24] [25]

1.4.2 Timeline of the CMB measurements

Since the discovery of the CMB in 1965, there have been many measurements of the cosmic microwave background radiation. We provide below a brief summary of the main experiments dealing with the CMB [26]:

- 1990 – The Cosmic Background Explorer satellite (COBE) – its measurements showed that the CMB has a nearly perfect black body spectrum
- 1992 – RELIKT - 1 – a soviet cosmic microwave anisotropy experiment - published results in January 1992 showed that there was detected the CMB anisotropy, three months before the announcement of the same fact by the COBE team
- 1999 – The BOOMERanG experiment – balloon-borne experiment which measured the CMB of a part of the sky during three sub-orbital balloon flights around the Antarctica. It was able to determine the geometry of the universe to be flat, because it made higher quality maps.
- 2003 – The Cosmic Background Imager (CBI) – is a radio telescope located in the Chilean Andes at the Chajnantor Observatory which produces high quality maps at high resolution of better than 0.1° , but covers small areas of the sky.
- 2003 – The Wilkinson Microwave Anisotropy Probe (WMAP) – produced the full-sky maps at resolution about 0.2° . Using them the WMAP team determined that the universe is 13.73 ± 0.12 billion years old and that a content of the universe presently consists of $(4.56 \pm 0.15)\%$ baryonic matter, $(22.8 \pm 1.3)\%$ dark matter and $(72.6 \pm 1.5)\%$ of dark energy that cause the universe to expand more faster.
- 2009 – The Planck spacecraft – is designed to produce the CMB anisotropy full-sky maps at higher resolution than WMAP. It is expected to announce its data in 2012.

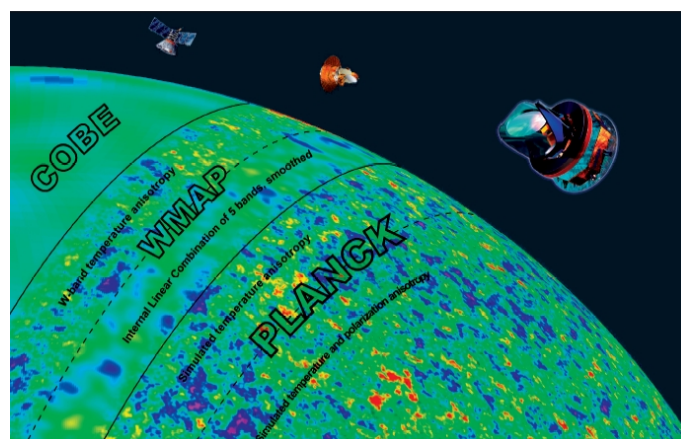


Figure 1.12: Comparison of the COBE, WMAP and Planck. (Figure adopted from web page of SciDAC.)

Chapter 2

A brief introduction to cosmology

Cosmology is the study of the universe as a whole. Its main goal is to answer the questions about the origin, age, current state, fate and shape of our universe. To achieve this, it uses various cosmological models which are confronted with the observations.

2.1 Foundations

The prevailing theory for the origin and evolution of the universe is now the Big Bang model. According to that, the entire space-time in the universe was created about 13.75 billion years ago from the extremely hot and dense state and has been expanding and cooling. The echo of the epoch of hot dense matter is the CMB which pervades the universe.

The Big Bang model is based on two foundations [28]:

- General Relativity – developed in 1916 by Albert Einstein as a new theory of gravity which generalizes the original theory of gravity created in 17th century by Isaac Newton. The main idea is that gravity is a distortion of space-time itself.
- The Cosmological Principle – the matter distribution in the universe is homogeneous and isotropic when averaged over large scales (from $\sim 10^8$ pc). The irregularities are local only.

2.2 Geometry of the universe

The matter, which is uniformly distributed in the universe, causes that the space-time is curved. That is why the matter influences a geometry of the universe, which is described by the parameter called the curvature:

- Positive curvature – the universe has a shape of a sphere and it is finite in extent, which means it has so-called closed topology
- Zero curvature – the universe is flat and it is infinite in extent, which is named as open topology
- Negative curvature – the universe has a shape of a saddle and it is also infinite in extent

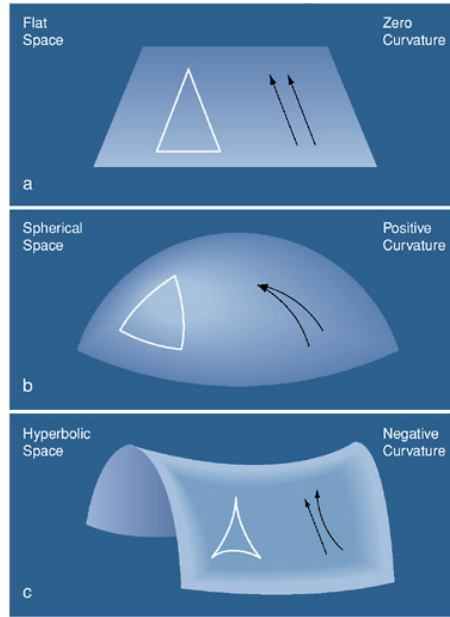


Figure 2.1: Curvature of the universe. (Figure adopted from web page of cosmology class lecture, University of Oregon.)

The curvature describes how the space-time is bent and it depends on how many matter is in the universe, which is expressed by term the average density of the universe. Very important term is so-called critical density of the universe, which is the mass/energy density of the universe capable of stopping the expansion of the universe after infinite time since Big Bang.[29]

The critical density (assuming zero cosmological constant Λ^1) is defined as:

$$\rho_{c,0} = \frac{3H_0^2}{8\pi G}, \quad (2.1)$$

where G is a gravitational constant and H_0 is a Hubble parameter. The present value of the critical density is $\rho_{c,0} = 9.47 \times 10^{-27} \text{kg} \cdot \text{m}^{-3}$. [27]

In addition, we define the density parameter Ω_0 as the ratio of the actual density of the universe to the critical density:

$$\Omega_0 = \frac{\rho_0}{\rho_{c,0}} = \frac{8\pi G\rho_0}{3H_0^2}. \quad (2.2)$$

This term can be also used to describe the geometry of the universe:

- $\Omega_0 > 1$ – the universe is closed and finite
- $\Omega_0 < 1$ – the universe is open and infinite
- $\Omega_0 = 1$ – the universe is flat and infinite

¹Cosmological constant was originally proposed by Albert Einstein to solve the equations for the static universe. It is considered now that the physical source for Λ is gravitationally repulsive dark energy.

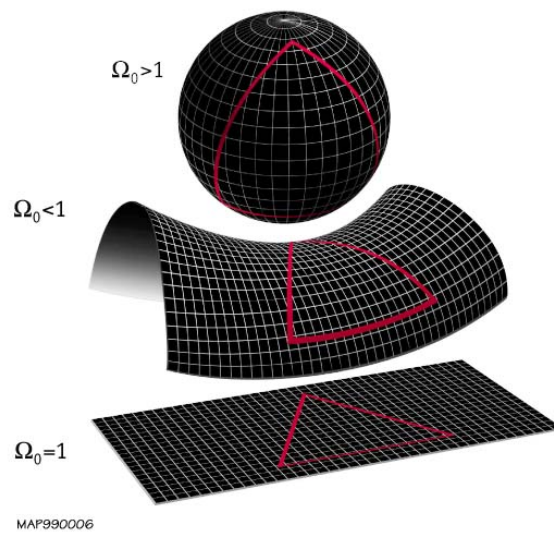


Figure 2.2: Geometry of the universe. (Figure adopted from web page of Atra Materia.)

2.3 Expansion

According to the Big Bang model the universe expands. Despite its name, the Big Bang was not any explosion. It was a creation of space and time itself everywhere in the universe, which began to expand. There is no center of expansion because the universe is expanding at all points. Although, we observe that all other galaxies are moving away from us, it does not mean that we are at the center of the universe. The observers from other galaxies could see the same situation. Furthermore, the expansion of the universe does not mean that all the objects in the universe are expanding. We observe, that the Earth, the solar system and even Galaxy are not expanding because they are held together by the gravity. The expansion applies to the objects which are not gravitationally bounded together like groups and cluster of the galaxies, which are moving apart.[30]

The details of the expansion, like its rate and from this resulting the fate of the universe depend on the density and the pressure of the universe. So, the evolution of the universe is determined by the fractional contribution of various types of matter [29]:

- Radiation – composed of photons and neutrinos, has a large positive pressure.
- Baryonic matter – it is an "ordinary matter" composed primarily of protons, neutrons and electrons. The pressure of baryonic matter can be negligible in cosmology.
- Dark matter – it is non-baryonic matter that interacts only weakly with ordinary matter and does not interact with the radiation. The pressure of dark matter can be also negligible.
- Dark energy – it is not known what it is exactly, but it could be a property of the vacuum itself. It has a large, negative pressure. Dark energy is represented by the cosmological constant Λ originally proposed by A. Einstein.

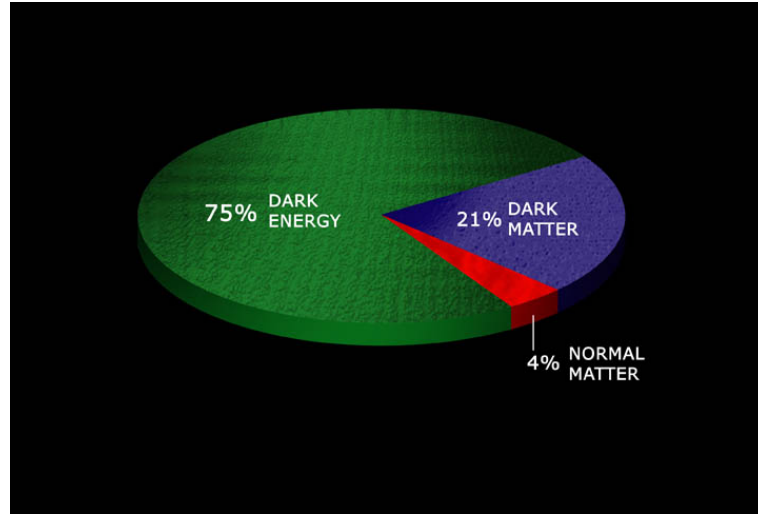


Figure 2.3: Present content of the universe. (Credit: NASA/CXC/M.Weiss)

Total density parameter Ω_0 can be expressed as a sum of mass densities of various types of matter:

$$\Omega_0 = \Omega_{m,0} + \Omega_{rel,0} + \Omega_\Lambda \quad (2.3)$$

$$\Omega_0 = \frac{8\pi G\rho_{m,0}}{3H^2} + \frac{8\pi G\rho_{rel,0}}{3H^2} + \frac{\Lambda c^2}{3H^2}, \quad (2.4)$$

where $\Omega_{m,0}$ is the current mass density of baryonic and dark matter, Ω_{rel} is the current equivalent mass density of the relativistic particles like photons and neutrinos and Ω_Λ is the effective mass density of the dark energy which stays constant in time.[31]

In the late 1920's Edwin Hubble measured radial velocities and the distances of the object called nebulae, and his measurements of Doppler shift showed that almost all galaxies were moving away from us. The recessional velocity v was directly proportional to the distance:

$$v = H_0 r, \quad (2.5)$$

where H_0 is the present Hubble constant, although it is not constant at all. The more appropriate term is the Hubble parameter because it varies with time. The most recent measurements of the Hubble constant using HST observations of Cepheid variables established its value at $H_0 = (70 \pm 7)$ km/s/Mpc.

The Hubble parameter can be also expressed as:

$$H(t) = \frac{\dot{R}(t)}{R(t)}, \quad (2.6)$$

where $R(t)$ is a dimensionless scale factor which describes the relative expansion of the universe. Its present value is $R(t_0)=1$.

As we can see, the Hubble parameter has a dimensions of inverse time, so by inverting the present value of the Hubble parameter, we can obtain so-called Hubble time t_H :

$$t_H = \frac{1}{H_0} \approx 13.8 \times 10^9 \text{ years}. \quad (2.7)$$

Note that the relation between Hubble time and the age of the universe depends on the history of the expansion rate, which is influenced by the density and the composition of the universe. For instance, for a flat universe composed mostly from matter, its age is $2/3H_0$. [32]

The expansion rate can be slowing down due to the gravitation force. It depends on the amount of matter in the universe. In addition, if there is a sufficient amount of matter, the gravity is strong enough to stop and even reverse the expansion. This would lead to the collapse of the universe. That is why we define the deceleration parameter $q(t)$: [33]

$$q(t) = -\frac{R(t)\ddot{R}(t)}{\dot{R}^2(t)} \tag{2.8}$$

According to the value of $q(t)$ there are several cases of expansion of the universe [34]:

- $q(t) > 1/2$ - the expansion is decelerating so quickly that universe can eventually collapse
- $q(t) < 1/2$ - the expansion is decelerating, but will continue forever
- $q(t) < 0$ - the expansion is accelerating (for models with Λ)

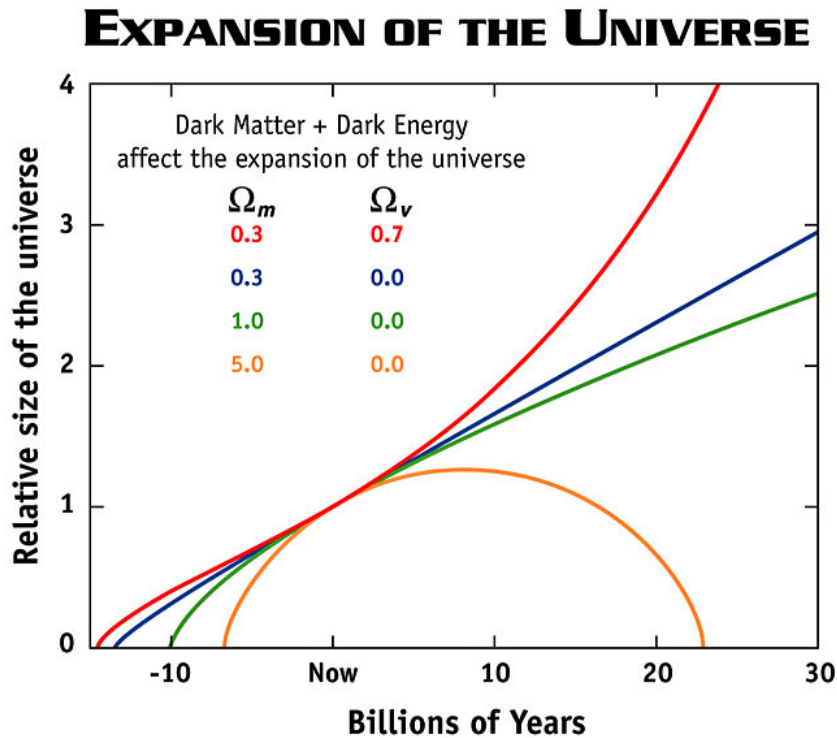


Figure 2.4: Expansion of the universe – scenarios. (NASA / WMAP Science Team)

At the Figure 2.4 there are depicted possible scenarios for the relative size of the universe vs. time [29]:

- green curve – a flat universe with the critical density, the expansion rate is continually slowing down
- blue curve – an open universe with the low density where expansion is slowing down, but not as much as the critical density universe because the pull of gravity is not as strong
- red curve – the universe where the expansion rate is accelerating due to the presence of dark energy (dark energy is the only kind of matter that can cause the expansion of the universe to accelerate). According to the recent observations we live actually in the universe which is represented by the this curve.

Chapter 3

WMAP

3.1 WMAP mission

The Wilkinson Microwave Anisotropy Probe (WMAP) is a space observatory designed to measure temperature and polarization anisotropies of the cosmic microwave background radiation. Due to its location at the L2¹ Sun – Earth point, which has stable thermal environment, it had the best observing conditions because Earth, Moon and Sun was always out of its detection field.

The goal of WMAP was to produce the full-sky CMB anisotropy maps with an angular resolution of at least 0.3° . In comparison with its predecessor COBE DMR mission, WMAP sky map data products are 45-times more sensitive and have 33-times larger angular resolution. By using these full-sky maps, WMAP science team was able to determine the content, evolution and the geometry of the universe.[35][36]

3.1.1 Mission timeline

Below is a list of the most important events in WMAP mission [37]:

- 1995 – WMAP was proposed to NASA as a MAP mission²
- June 30, 2001 – launch of the WMAP from the Cape Canaveral
- August 10, 2001 – arrival of the WMAP to the L2 point, which is used as a permanent observing location
- April 2002 – completion of the first full sky observation
- February 2003 – first-year data release
- March 2006 – three-years data release

¹L2 is one of the five Lagrange Points, which mark positions where the gravitational pull of the two large masses precisely equals the centripetal force required to rotate with them. For more information, see http://map.gsfc.nasa.gov/mission/observatory_l2.html.

²The original name MAP was later in 2003 changed to WMAP in honor of cosmologist David Todd Wilkinson, who participated in the mission.

- March 2008 – five-years data release
- January 2010 – seven-years data release
- August 19, 2010 – WMAP ended the science observations
- 8 September 2010 – WMAP moved from the L2 point to the heliocentric orbit
- 28 October 2010 – reception of the last command, since that WMAP has been collecting data in silence and will keep it depending on the battery durance

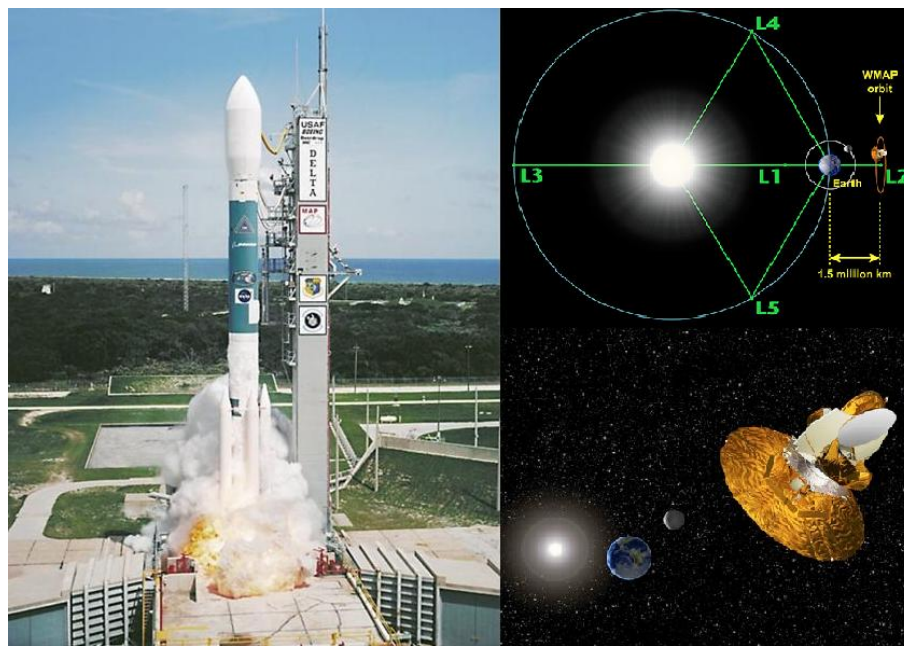


Figure 3.1: Collage image of launch, L2 position and an artist impression of the WMAP. (NASA / Kennedy Space Flight Center / WMAP Science Team)

3.1.2 Technical specification

WMAP is the medium-class size spacecraft with the mass about 840 kg. The most significant part of the spacecraft is a solar panel with a diameter of 5 m that shades the WMAP instruments during observations and supplies the electricity for the entire probe. Upon the panels there are the systems supporting the mission like the electronics, pointing and control system, power services and a hydrazine propulsion system consisting of 8 thrusters. At a top deck is the WMAP instrument which does the scientific observations.

The WMAP instrument consists of two components: the optics and the radiometers. Optical system comprises a pair of two Gregorian telescopes with a size of the primary reflectors of 1.4×1.6 meter which focus the microwave radiation, which comes from two different spots on the sky in the focal plane. Focused signal is then measured by 20 differential radiometers which are cooled to approximately 90 K and cover 5 frequency bands.[36] Further WMAP instrument specification is provided at the table.[35][36][38]

Frequency band	K	Ka	Q	V	W
Frequencies (GHz)	22	30	40	60	90
Wavelengths (mm)	13.6	10.0	7.5	5.0	3.3
Bandwidth (GHz)	5.5	7.0	8.3	14.0	20.5
Resolution (FWHM, degrees)	0.93	0.68	0.53	0.35	<0.23
Sensitivity (μK , $0.3^\circ \times 0.3^\circ$ pixel)	~ 35				
Number of Differencing Assemblies (DA)	1	1	2	2	4
Number of Radiometers	2	2	4	4	8

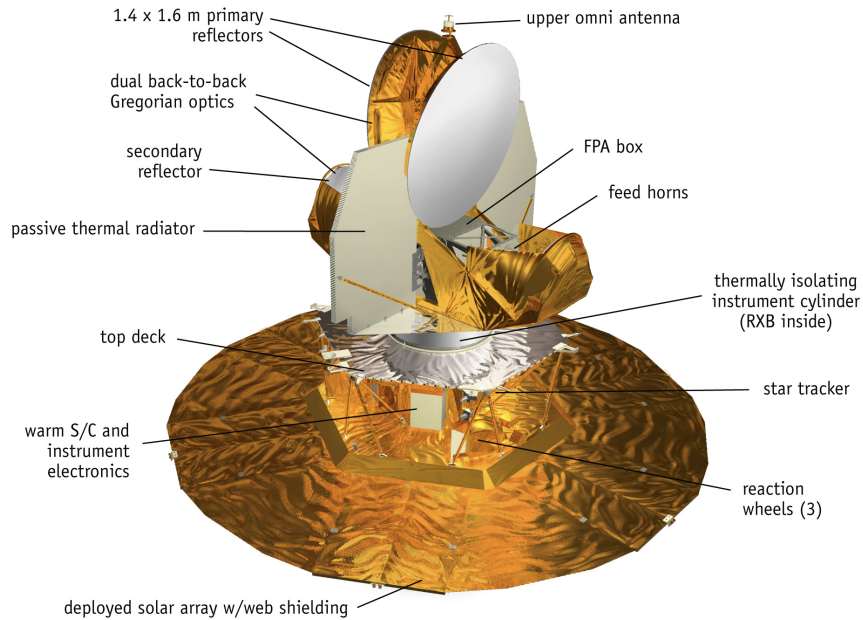


Figure 3.2: Descriptive image of the WMAP. (NASA / WMAP Science Team)

3.1.3 Observations

WMAP spacecraft was observing the CMB at the L2 Lagrange point which is about 1.5 million km far from Earth. This observing site provided ideal conditions for the CMB observations due to its distance from Earth, which minimizes possible disturbances like Earth microwave emission, magnetic fields etc.[36]

The WMAP was launched to observe full-sky in microwave region of the electromagnetic spectrum. In addition, for better determination of the statistical properties of the universe, cosmologists need as much sky samples as possible. The more sky samples they have, the more accurate constraints of the cosmological models they can determine. Scan strategy was generally designed to reject the systematic errors. Its main goals are [39]:

- Scan a large fraction of the sky as rapidly as possible considering the technical capabilities of spacecraft.
- Scan each sky pixel through as many azimuth angles as possible.
- Scan a given pixel on as many time scales as possible.
- Keep the instrument in permanent shade due to the passive cooling and avoidance of signals from the Earth, Moon and Sun.

The WMAP scan strategy allowed probe to cover about 30% of the sky each day. Because L2 point follows the Earth around the Sun, and thereby WMAP orbited the Sun, it achieved the full-sky coverage every six months.[36] This produced the full-sky maps every six months which were compared for consistency and also provided stability check of the observations. For the better illustration see Figure 3.3 below.

WMAP was a differential experiment, which means that it measured the temperature differences between two points on the sky. The temperature or more exactly brightness temperature³ T_B is defined for a black body by the equation [41]:

$$I_\nu = B_\nu(T_B), \quad (3.1)$$

where I_ν is the specific intensity and B_ν is given by the Planck's law (mentioned in Section 1.1):

$$B_\nu = \frac{2h\nu^3}{c^2} \frac{1}{e^{\frac{h\nu}{k_B T_B}} - 1}. \quad (3.2)$$

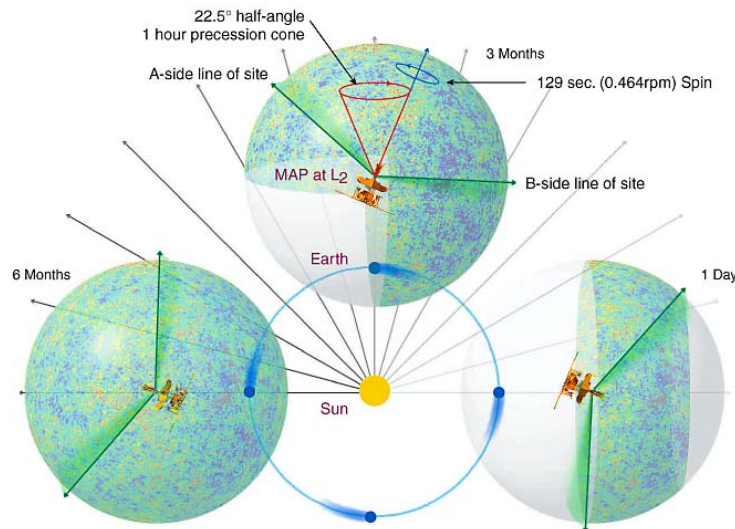


Figure 3.3: WMAP coverage. (NASA / WMAP Science Team)

³The temperature that a blackbody would need to have in order to emit radiation of the observed intensity at a given wavelength. [40]

3.2 Data products and software

WMAP team provides several data products and software which are publicly available on LAMBDA archive⁴. It is containing the data from the four data releases (in 2003, 2006, 2008 and 2010). In bachelor thesis we used the seven-years data from release published in January 2010.

3.2.1 Sky maps

The WMAP sky maps are the crucial data product for the CMB analysis. That is why the LAMBDA site provides several types of the sky maps at three resolutions: Res 4 (NSide=16), standard Res 9 (NSide=512) and Res 10 (NSide=1024). In general, the seven-year release contains:

- Full resolution single year sky maps – produced using a single year of data
- Full resolution co-added seven year sky maps – constructed using a mean of the seven single years maps
- Reduced resolution sky maps – the low resolution maps (NSide=16)

From the vast LAMBDA Legacy archive, you can download these maps in various frequency bands (K, Ka, Q, V, W) or differencing assemblies (K1, Ka1, Q1, Q2, V1, V2, W1, W2, W3, W4). Furthermore, there are also smoothed maps (to 1° resolution) and foreground reduced maps.[42][43]

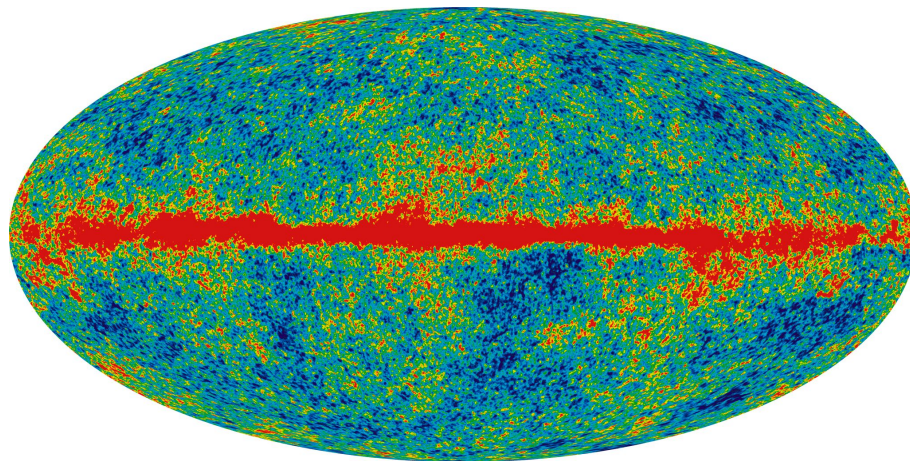


Figure 3.4: Full-sky temperature map in W-Band (94 GHz). (NASA / Science Team)

All WMAP sky maps are supplied in FITS binary table format using nested HEALPix⁵ pixel ordering scheme in Galactic coordinates⁶ (Subsection 3.2.4). The row in the table

⁴LAMBDA is an acronym for Legacy Archive for Microwave Background Data Analysis and it is available on website <http://lambda.gsfc.nasa.gov/>.

⁵<http://healpix.jpl.nasa.gov>

⁶You can retrieve the galactic coordinates for each pixel using FITS file available on http://lambda.gsfc.nasa.gov/toolbox/tb_pixelcoords.cfm.

represents a single pixel and the number of rows depends on the map resolution. The number of columns depends on the what the map includes. For the temperature maps (they do not contain polarization data), which we used, the columns are [44]:

- TEMPERATURE – temperature in mK (Stokes I)
- N_OBS – the effective number of observations

A more detailed description of maps formatting is available on http://lambda.gsfc.nasa.gov/product/map/dr4/skymap_file_format_info.cfm.

3.2.2 Foreground exclusion masks

To exclude the portions of the sky, which are contaminated by the foreground emission, we used the exclusion pixel masks supplied by LAMBDA at the section "Ancillary data". They mainly excludes sky area in the Galactic plane region, where is observed the majority of the foreground emission. They are based on the Model of the Galactic foreground emission (described in Bennett et al. (2003)), which was determined by analysing of all 5 WMAP frequency bands. According to this model, the emission from our Galaxy is minimal between V and W band. Furthermore, they concluded that the emission is due to by three distinct emission components [44]:

- Synchrotron emission from interaction of relativistic electrons with magnetic field.
- Thermal emission from interstellar dust grains.
- Free-free emission from the ionized interstellar medium.

LAMBDA provides for temperature analysis two types of masks which exclude different portion of the sky:

- the standard cut (12% cut) , KQ85
- the extended cut (29% cut), KQ75

These masks are in the FITS format, using HEALPix nested scheme in Galactic coordinates, just like the sky maps. LAMBDA supplies the exclusion masks in two resolutions: NSide=512 and NSide=1024. The mask data file contains N_OBS field, where are the mask values for each pixel. They are either zero or one. If the value is zero, the pixel is rejected, and if the value is one, the pixel is accepted.[45]

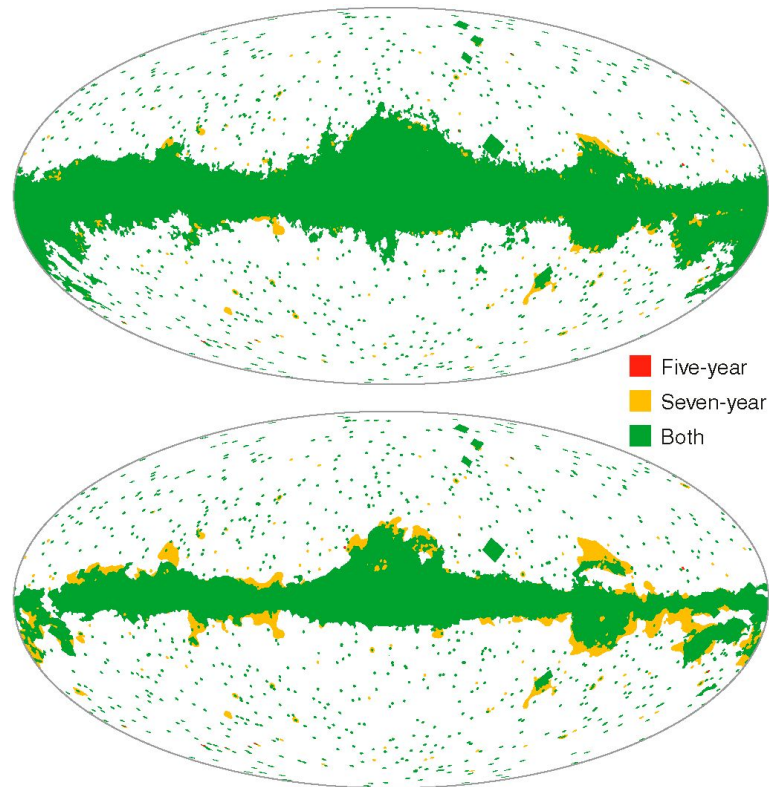


Figure 3.5: Comparison of two seven-year masks to five-year masks. At the top is compared KQ75 with KQ75y7, and at the bottom KQ85 with KQ85y7. (NASA / WMAP Science Team)

3.2.3 Beam transfer functions

For interpreting data from CMB experiments, it is important to know the beam profiles which were determined by observing the Jupiter. Beam transfer functions for each DA were computed by WMAP Science Team from the Legendre transform of the beam profiles. To reveal the intrinsic angular power spectrum on the sky, we divided the output power spectrum by the window function, of which part is the beam transfer function.

LAMBDA archive provides in the ASCII tables beam transfer function for each DA. In the first column is the multipole moment l and in the second one is the square of the beam transfer function normalized to 1.0 at $l=1$.[\[44\]](#)

3.2.4 HEALPix

An acronym HEALPix stands for Hierarchical Equal Area isoLatitude Pixelization of a sphere. This pixelization has two main features [46]:

- It divides the surface of a sphere to the areas of pixels which are identical.
- Distribution of pixels is iso-latitude which means that the pixels are located in the lines of a constant latitude.[44]

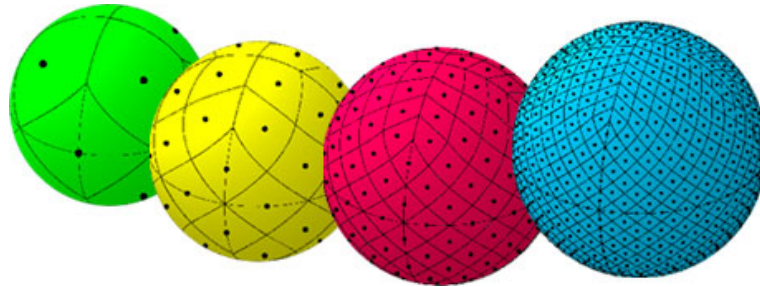


Figure 3.6: A comparative image of HEALPix grid in different resolutions. The green sphere has the lowest resolution possible where the sphere is divided into 12 equal sized pixels. The resolution of yellow sphere is 48 pixels, red sphere has a grid of 192 pixels, and the blue sphere is partitioned into 768 pixels. (NASA / HEALPix)

To evaluate the cross-power spectra from WMAP sky maps we used the HEALPix facility Anafast. It performs a harmonic analysis of one or two sky maps in binary FITS format. The output is ascii FITS file containing angular cross-power spectrum from two independent sky maps. In addition, it offers possibility of writing the a_{lm} coefficients to another FITS file.

Anafast was also used to subtract the foreground emission using exclusion masks before the harmonic analysis. The whole description of Anafast features is available on <http://healpix.jpl.nasa.gov/html/facilitiesnode7.htm>.

Chapter 4

Analysis of CMB angular power spectrum

4.1 Angular power spectrum

The CMB temperature fluctuations are usually specified by the angular power spectrum. It is computed from the full-sky maps which carry information about the CMB temperature anisotropies. Estimation of the angular power spectrum is crucial for setting the constraints on parameters of various cosmological models.

4.1.1 Estimation

To estimate the angular cross-power spectrum we used a similar approach as described in Hinshaw et al. (2003)[47], which is actually the same thing as explained in Section 1.3 At first, we take the CMB maps containing fluctuations of the brightness temperature $\Delta T(l, b)$, which are on the specific position (l, b) , perform the spherical transform on them and get the expansion coefficients a_{lm} from each map. Then we determine the angular cross-power spectrum from these two maps from different DA using the equation (1.8), recall:

$$C_l = \frac{1}{2l+1} \sum_{m=-l}^l a_{lm}^i a_{lm}^{j*}, \quad (4.1)$$

where coefficient a_{lm}^i is evaluated from map i and a_{lm}^j from different map j . The advantage of using cross-power spectrum is the fact, that the equation (4.1) provides an unbiased estimation of the power spectrum C_l , if the noise between two maps is uncorrelated.

4.1.2 Bias of the CMB power spectrum estimation

Although we can determine the angular power spectrum directly from the particular maps using equation (4.1), we have to consider the fact that the all realistic measurements of CMB anisotropies contain many sources of errors. In this section we describe the effects of the exclusion of Galactic foreground emission and instrumental effects.

As we already know from the previous sections, the real WMAP full-sky maps are contaminated by the emission from our Galaxy and from extragalactic sources. For this

reason it is necessary to subtract this emission from our data, so we can use for CMB power spectrum estimation only a fraction of the sky. This can be achieved by using the exclusion masks described in Subsection 3.2.2.

We must also consider the effects of the instrumental errors. Thus the CMB power spectrum is affected by the instrumental properties themselves, for example by finite resolution and instrumental noise. These errors also appear in the pixelized data on the sky maps.

To describe the effects of bias of power spectra due to the instrument and incomplete sky coverage we used again the similar method which is described in G. Hinshaw et al. (2003)[47]. The cross-power spectrum C_l^{ij} which is evaluated from two sky maps measured in differencing assembly (DA) i , and j respectively, is for simplicity rewritten in a form of $C_l^{\mathbf{i}}$, where we only changed the pair of indexes i, j as $\mathbf{i} \equiv (i, j)$. Now the angular power spectrum has a form:

$$C_l^{\mathbf{i}} = w_l^{\mathbf{i}} C_l + N_l^{\mathbf{i}}, \quad (4.2)$$

where $N_l^{\mathbf{i}}$ is a noise spectrum and $w_l^{\mathbf{i}}$ is the window function which can be expressed as:

$$w_l^{\mathbf{i}} = b_l^i b_l^j p_l^2, \quad (4.3)$$

where b_l^i stands for the beam transfer function for differencing assembly \mathbf{i} and p_l is a pixel transfer function which is supplied with the HEALPix package.

The relation between underlying angular power spectrum and cross-spectrum can be rewritten in form using average of the observed angular cross-power spectrum (and average of noise spectrum) which estimates true power spectrum C_l as:

$$\langle C_l^{\mathbf{i}} \rangle = w_l^{\mathbf{i}} C_l + \langle N_l^{\mathbf{i}} \rangle \delta_{ij}. \quad (4.4)$$

As mentioned in previous subsection, we can calculate the unbiased estimation of power spectrum using the cross-power spectrum evaluated from different maps, if noise between them is uncorrelated. That is why we used the maps from the statistically independent channels or DAs. In addition, we see that the Kronecker symbol indicates that between two DAs ($i \neq j$) the noise is uncorrelated, so the noise bias term is $\langle N_l^{\mathbf{i}} \rangle = 0$:

$$\langle C_l^{\mathbf{i}} \rangle = w_l^{\mathbf{i}} C_l = b_l^i b_l^j p_l^2 C_l. \quad (4.5)$$

Due to this advantage, we used several cross-power spectra, each computed from two DAs maps to determine the desired CMB power spectrum C_l .

Because we used the exclusion mask for the subtraction the Galactic foreground emission, for estimation of angular power spectrum we did not use the whole sky, but only a fraction. This is represented by the factor f_{sky} , which we added to the window function:

$$w_l^{\mathbf{i}} = f_{\text{sky}} b_l^i b_l^j p_l^2, \quad (4.6)$$

and finally, using the cross-power spectrum we can estimate the underlying angular power spectrum C_l in case of reduced sky coverage as:

$$\langle C_l^{\mathbf{i}} \rangle = f_{\text{sky}} b_l^i b_l^j p_l^2 C_l. \quad (4.7)$$

In addition, due to the f_{sky} factor, the uncertainty δC_l is now [48]:

$$\delta C_l = \sqrt{\frac{2}{(2l+1)f_{\text{sky}}}}. \quad (4.8)$$

4.2 Interpretation of acoustic peaks

As we know from Section 1.3, the angular power spectrum, which is actually a graph of average intensity of temperature fluctuations on different angular scales, contains several acoustic peaks due to the acoustic waves which were propagating across the primordial plasma before decoupling. In this section we will describe how they help cosmologist to answer some questions concerning the matter content and the curvature of the universe.

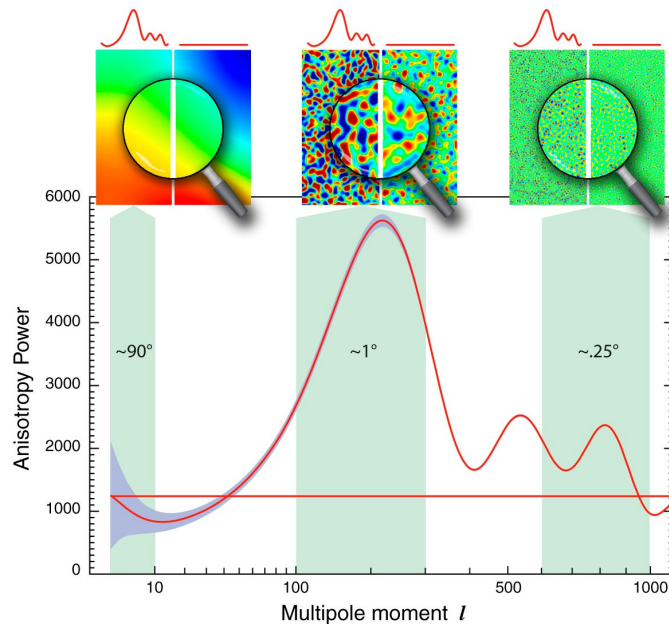


Figure 4.1: Angular power spectrum of temperature fluctuations. In a graph are two scenarios – the straight line represent a true uniform temperature distribution and the curve above the line is the actual sky measurement. (NASA/WMAP Science Team)

Because the acoustic oscillations are just periodic density variations of hot dense plasma, the CMB photons released during decoupling inform us about a phase of the acoustic oscillation at that very moment. Due to different wavelength (and thereby the size of density perturbation), their phases were different at the time of decoupling. Especially the interesting are those waves which were at the maxima when the matter and radiation decoupled – they correspond to the peaks in the CMB temperature angular power spectrum. On the other hand, the troughs between the peaks correspond to the waves which had the intermediate phase between two extrema at the recombination.[49]

The first acoustic peak correspond to the acoustic wave with the largest possible wavelength, and thereby the size of density perturbation, which is maximally compressed for the first time at the decoupling. The largest possible wavelength depends on the so-called sonic horizon distance (or sound horizon), which is a size of the largest casually connected region, so its a distance that a acoustic wave could have traveled since the end of inflation till the time of decoupling.

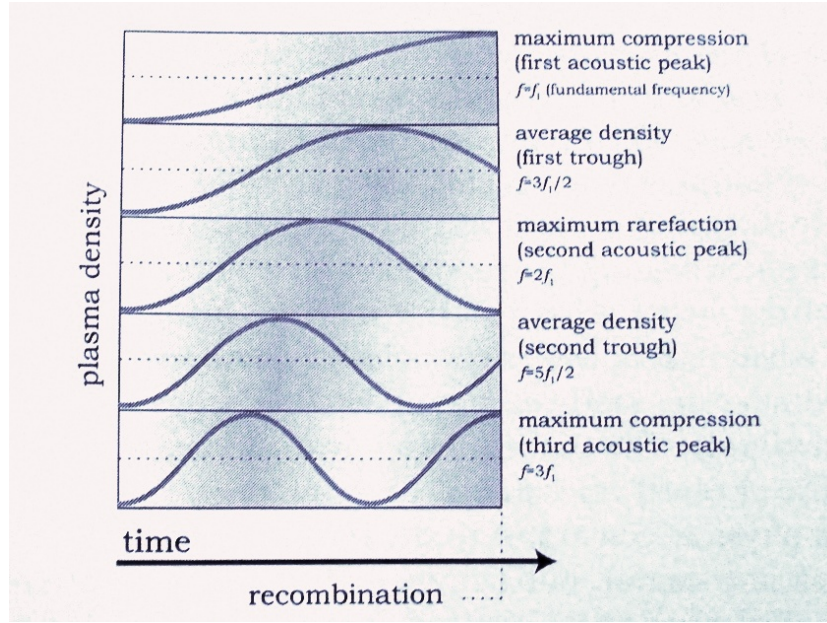


Figure 4.2: Phases of the acoustic waves with different frequency at the decoupling. (Figure adopted from Amedeo Balbi: The music of the Big Bang.)

The angular diameter of sound horizon is defined as:

$$\theta = \frac{r_s(t_{\text{dec}})}{r_a(t_{\text{dec}})}, \quad (4.9)$$

where $r_s(t_{\text{dec}})$ is sonic horizon distance at the decoupling and $r_a(t_{\text{dec}})$ is a comoving angular diameter distance to the surface of the last scattering. They both depend on the cosmological parameters and various cosmological models, which we are not going to describe in this bachelor thesis. Just for the information, the values from Ostlie, Dale A. and Carroll, Bradley W: An Introduction to Modern Astrophysics [14] are $r_s(t_{\text{dec}}) = 6.2 \times 10^{21} \text{ m} = 200 \text{ kpc}$ and (after short calculation) $r_a(t_{\text{dec}}) = 3.5 \times 10^{23} \text{ m}$. So the angular diameter is $\theta = 1.03^\circ$ and the first acoustic peak is at $l \approx \pi/\theta \approx 175$.

The location of the first acoustic peak is influenced by the spatial curvature of the universe, so it implies the value of total density parameter Ω_0 . As shown at the Figure 4.3, the observed angular size of the spot depends on the geometry of the universe, due to the gravity which bends the lights coming from the surface of the last scattering. The bending of CMB photons depends on how the universe is curved, thus on the total density of matter and energy described by Ω_0 . We can calculate the size of the spot using theoretical models. Then we just compare the calculated diameter size of the spot with the observed one and determine the curvature and thereby Ω_0 . Because the angular size of the spot is related to the position of the first peak, we can determine the Ω_0 parameter by finding the first peak location. According to Heller, Michael and Woodin, W. Hugh. Infinity: New Research Frontiers [50] calculations show that the position of the first peak is:

$$l \simeq 220/\sqrt{\Omega_0}. \quad (4.10)$$

So for the flat universe the first peak occurs at $l \simeq 220$. If the universe is closed, then the first peak is at $l < 220$, and in case of open universe the first peak is located at $l > 220$.

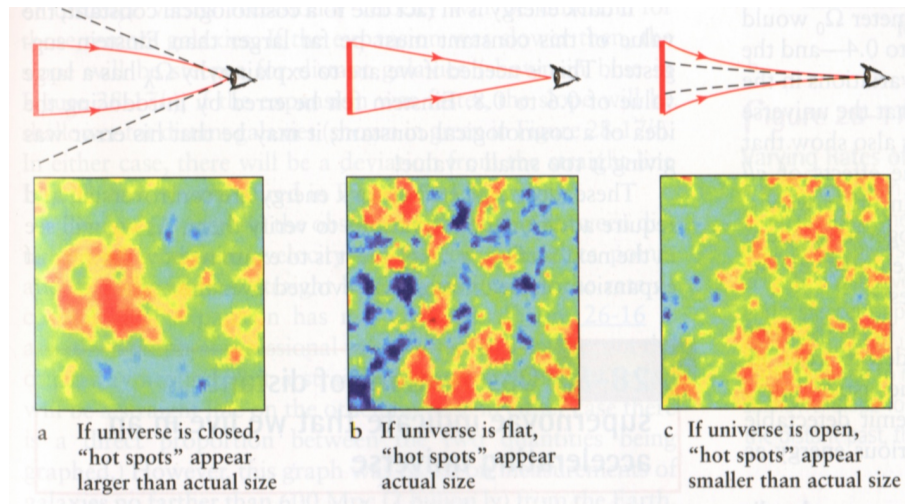


Figure 4.3: The curvature and the propagation of light – consequences. (Figure adopted from online cosmology class lectures at Institute of Astronomy, National Tsing Hua University, Hsinchu, Taiwan.)

There are also another peaks which correspond to the sound wave with the wavelength equal to the integer fraction of the largest one, which is responsible for the first peak. In general, the even peaks are due to the acoustic oscillations caught at the rarefaction, while the odd peaks represent the waves which are maximally compressed. So the second acoustic peak is caused by the oscillation of the acoustic wave, which underwent the maximum compression and it was maximally rarefied at the decoupling. The third acoustic peak occurred when acoustic wave was maximally compressed for the second time, when the CMB photons were released.[49]

We can also see, that these peaks have different heights. They depend on the quantity of matter – both baryonic and non-baryonic, which is usually called dark matter. They played different roles in the mechanism of acoustic oscillations –both caused the collapse of the density perturbation due to the gravity, but only baryonic matter participated in the oscillations, because dark matter do not interact with photons and thus was not influenced by radiation pressure. That is why the peaks corresponding to the compression due to the gravity are relatively higher than those which represent the rarefaction of the acoustic wave. So the relative heights of the acoustic peaks can consequently specify the amount of baryonic and dark matter.[49]

Chapter 5

Results

5.1 From sky maps to power spectra

In this section we present our results – angular power spectra obtained from the full-sky maps. As our primary data source we used the 7-year co-added full-sky maps of CMB anisotropies with resolution of Res 9 from LAMBDA. As previously mentioned, if the noise is uncorrelated between two DAs, using cross-power spectrum we can neglect noise term in equation (4.4). For this reason we computed cross-power spectra and we used maps from maps in V and W band, because of its resolution. So we got 8 cross-power spectra determined from maps: V1W1, V1W2, V1W3, V1W4, V2W1, V2W2, V2W3, V2W4. Furthermore, during calculation, we subtract the foreground emission using exclusion mask – KQ75 mask, after which is used for estimation 71% of the sky. The resultant cross-power spectra were derived using the HEALPix (K.M. Górski et al., 2005, ApJ, 622, p759) package.

The next step was to correct the obtained cross-power spectra C_l^i from each DA for the effects of beam, pixel window and exclusion mask, so they were divided by window function. Finally, we plotted the angular cross-power spectrum in the form $l(l+1)C_l/2\pi$. At the Figure 5.1 below is depicted the effect of the window function on the final cross-power spectrum. Because this process is analogous for every DA (although, each DA has different beam transfer function and thereby window function), we provide the comparison only for one cross-power spectrum – V1W1.

As we already know, estimation of power spectrum is affected by the uncertainty due to the cosmic variance. Because it is dominant source of an error only at low multipoles up to $l \sim 350$ [47] and it is a quite unaesthetic to depict the whole graph of cross-power spectrum with error bars due to cosmic variance, we provide the graph at lower multipoles with one-sigma error bars for cosmic variance, and sky coverage calculated using equation (4.12).

There are also the other sources of the errors, mainly due to uncertainties in beam transfer functions, imperfect foreground exclusion masks and absolute calibration uncertainty of WMAP described in Hinshaw et al. (2003)[47]. Because in this thesis we do not intend to make a combined power spectrum from calculated cross-power spectra, and because of the complexity of calculating these errors, we simply plotted our results for each combination of DA in graphs, and see, that these power spectra are almost the same.

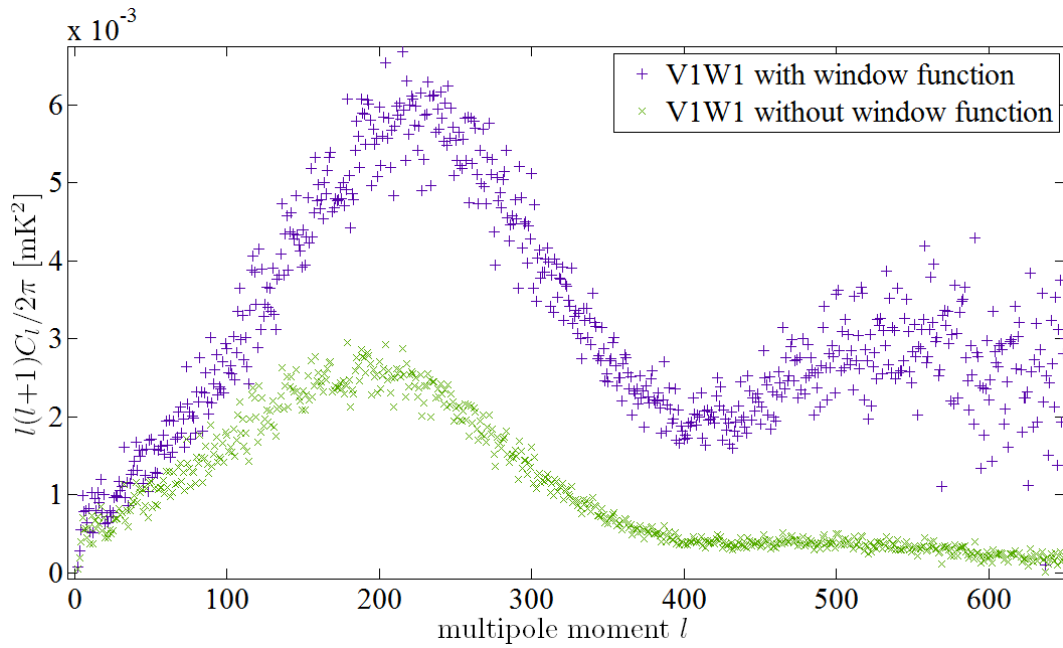


Figure 5.1: The effect of window function.

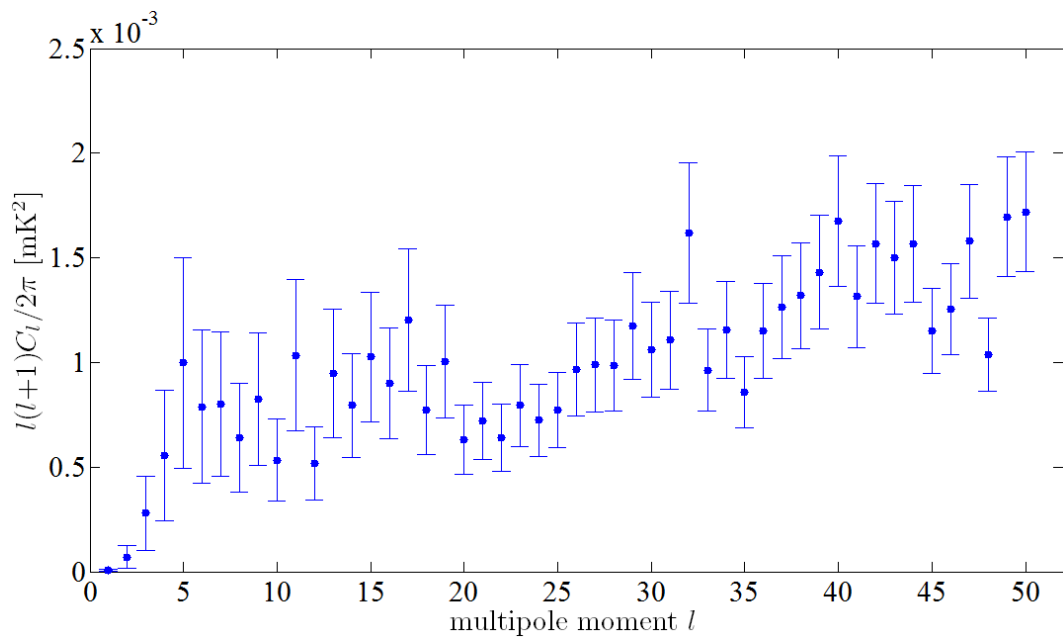


Figure 5.2: Cosmic variance uncertainty at lower multipoles using in cross-power spectrum V1W1.

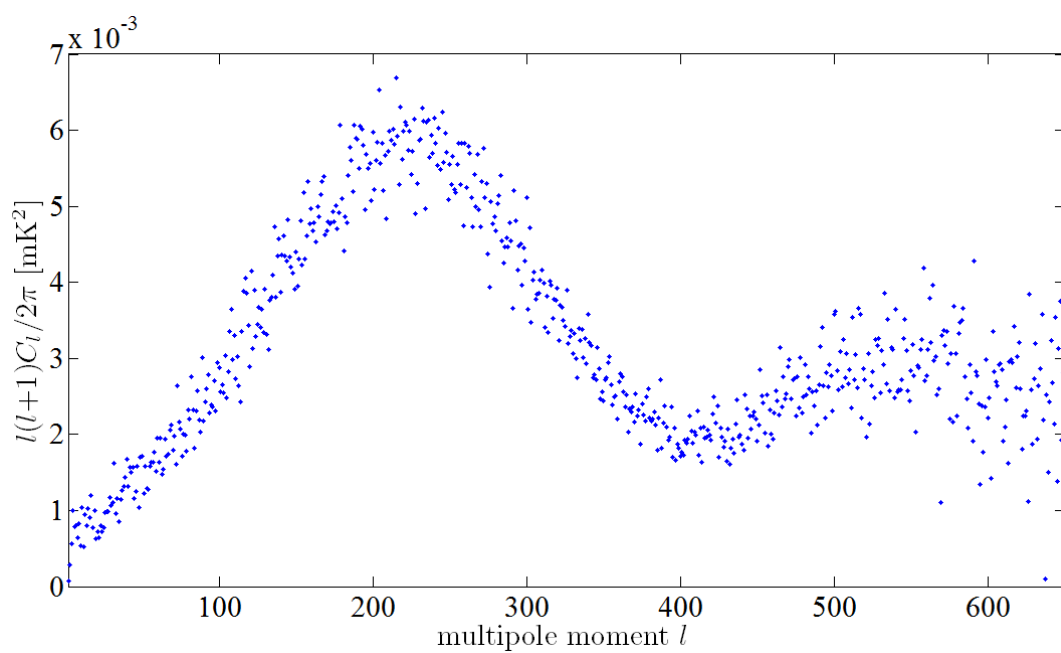


Figure 5.3: Cross-power spectrum V1W1.

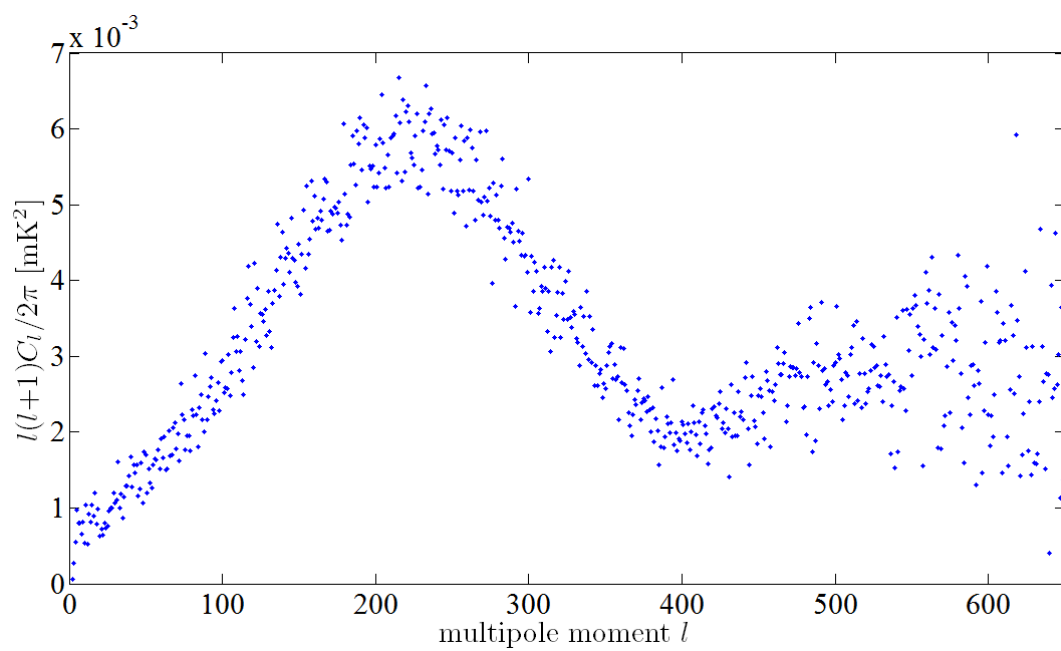


Figure 5.4: Cross-power spectrum V1W2.

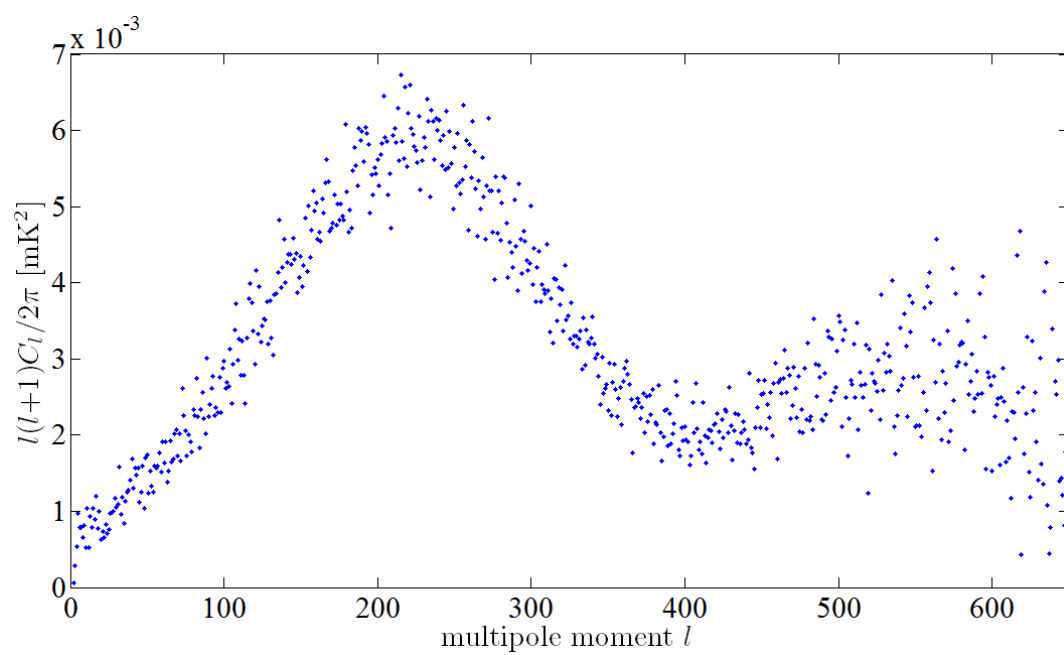


Figure 5.5: Cross-power spectrum V1W3.

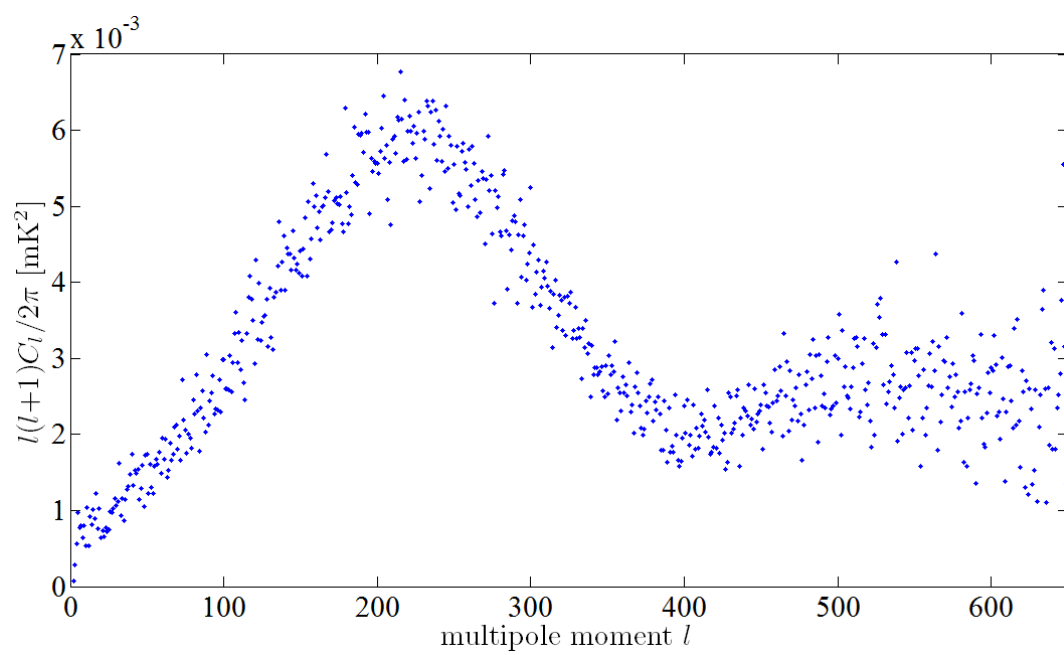


Figure 5.6: Cross-power spectrum V1W4.

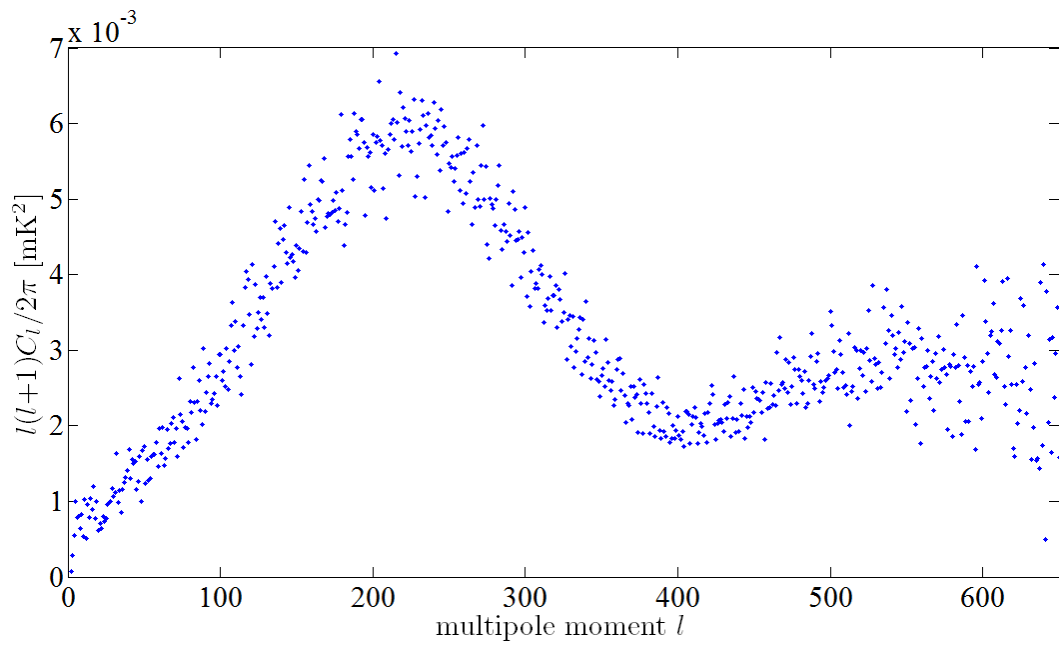


Figure 5.7: Cross-power spectrum V2W1.

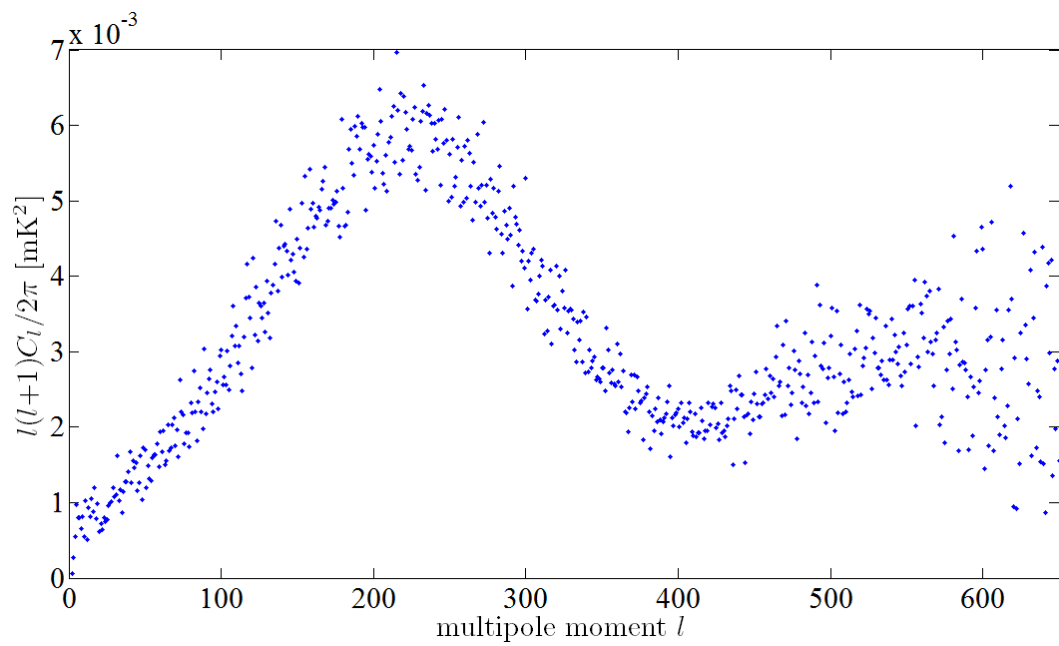


Figure 5.8: Cross-power spectrum V2W2.

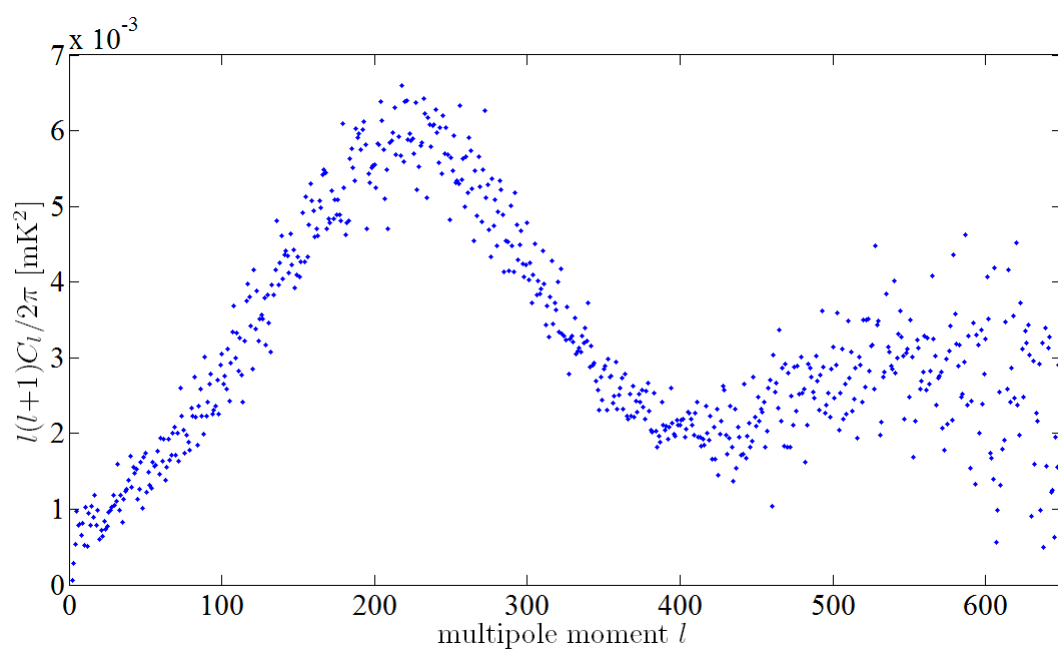


Figure 5.9: Cross-power spectrum V2W3.

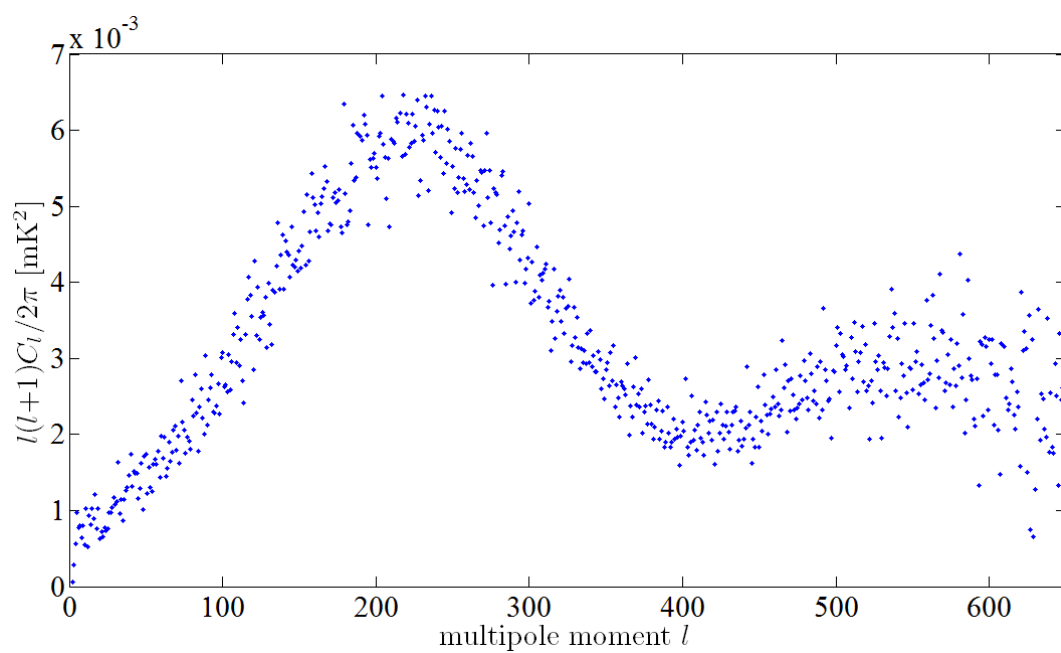


Figure 5.10: Cross-power spectrum V2W4.

5.2 Fitting

In this section we present a basics of spherical harmonics and Legendre polynomials which result in fact that they can be used for fitting our angular power spectrum. Recall the equation (1.8) from Section 1.3:

$$C_l = \frac{1}{2l+1} \sum_{m=-l}^l |a_{lm}|^2. \quad (5.1)$$

We see that it is an average of a_{lm} coefficient over the ensemble. These spherical expansion coefficients we can define as (assuming the galactic coordinates l, b) [51]:

$$a_{lm} = \int_0^{2\pi} dl \int_0^\pi \sin(b) \Delta T(l, b) Y_{lm}^*(l, b) db, \quad (5.2)$$

where $Y_{lm}^*(l, b)$ is the complex conjugate of the spherical harmonic function which can be defined using associated Legendre polynomials [52]:

$$Y_{lm}(l, b) = (-1)^m \sqrt{\frac{2l+1}{4\pi} \frac{(l-m)!}{(l+m)!}} P_{lm} e^{imb}. \quad (5.3)$$

They are related to the ordinary Legendre polynomials as a function of x by equation [52]:

$$P_{lm} = (-1)^m (1-x^2)^{m/2} \frac{d^m}{dx^m} P_l. \quad (5.4)$$

The first eight Legendre polynomials are (from order $l=0-7$) [15]:

$$\begin{aligned} P_0(x) &= 1 \\ P_1(x) &= x \\ P_2(x) &= \frac{1}{2}(3x^2 - 1) \\ P_3(x) &= \frac{1}{2}(5x^3 - 3x) \\ P_4(x) &= \frac{1}{8}(35x^4 - 30x^2 + 3) \\ P_5(x) &= \frac{1}{8}(63x^5 - 70x^3 + 15x) \\ P_6(x) &= \frac{1}{16}(231x^6 - 315x^4 + 105x^2 - 5) \\ P_7(x) &= \frac{1}{16}(429x^7 - 693x^5 + 315x^3 - 35x). \end{aligned}$$

As we can see, due to the relation of angular power spectrum to the Legendre polynomials, we can use them for fitting, which is basically based on a decomposition of function $f(l) = l(l+1)C_l/2\pi$ in Legendre polynomials:

$$f(l) = \sum_{i \geq 0} a_i P_i(l), \quad (5.5)$$

where a_i is a coefficient. However, we need to expand our function only to the order i when a product $a_i P_i(l)$ is still larger than the root mean square error (RMSE) of our fit. Generally, the product $a_i P_i(l)$ would have to be evaluated for every l and then compared with RMSE. However, we are mainly interested in position of the first acoustic peak (which is at $l \approx 220$), so in table on the next page are the values of the products $a_i P_i(220)$. This table

also contains the calculated coefficients (with their uncertainty) of the expansion of $f(l)$ in Legendre polynomials used for fitting with $\text{RMSE} = 4.0 \times 10^{-4} \text{mK}^2$, and the number of fitted values was $N=650$. For that procedure we used least squares method implemented in MATLAB¹. Because the power spectra evaluated from different maps are almost the same, we fitted the cross-power spectrum which seemed to be the most suitable for fitting, which is from maps V2 and W4.

Legendre polynomial	coefficient	value [mK^2]	$a_i P_i(220)$ [mK^2]
P_0	a_0	$(6.37 \pm 1.27) \times 10^{-4}$	6.37×10^{-4}
P_1	a_1	$(1.56 \pm 0.70) \times 10^{-5}$	3.43×10^{-4}
P_2	a_2	$(-1.44 \pm 0.83) \times 10^{-7}$	-1.04×10^{-2}
P_3	a_3	$(2.26 \pm 0.39) \times 10^{-9}$	6.01×10^{-2}
P_4	a_4	$(-8.64 \pm 0.92) \times 10^{-12}$	-8.86×10^{-2}
P_5	a_5	$(1.33 \pm 0.11) \times 10^{-14}$	5.39×10^{-2}
P_6	a_6	$(-9.02 \pm 0.66) \times 10^{-18}$	-1.48×10^{-2}
P_7	a_7	$(2.26 \pm 0.16) \times 10^{-21}$	1.51×10^{-3}

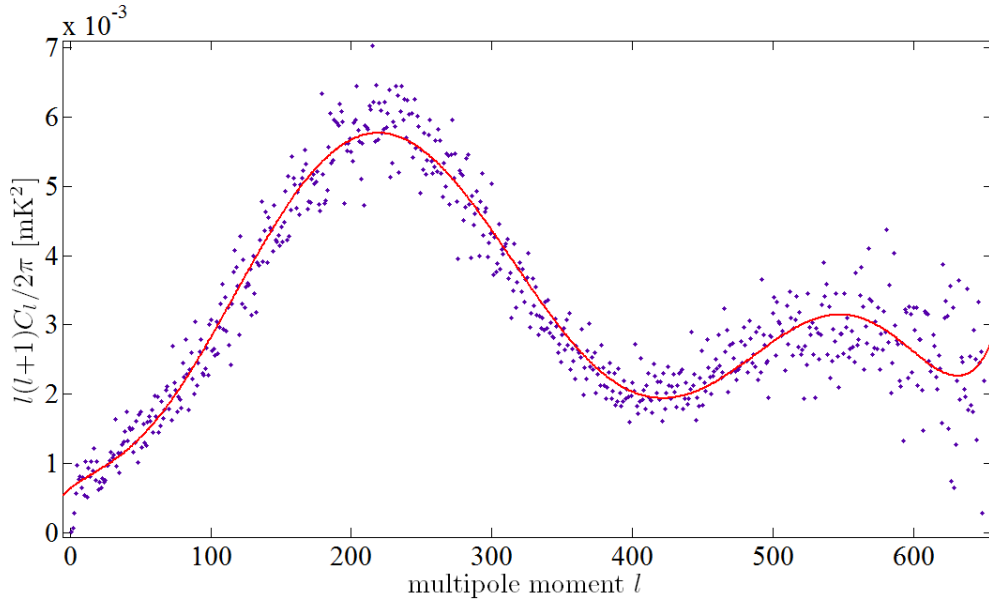


Figure 5.11: Fitting of cross-power spectrum V2W4.

The fitting of the power spectrum gives us the positions of two acoustic peaks. The first acoustic peak is located at $l=219.3$ and the second one is at $l=547.2$. Because the uncertainty estimation requires more complex least squares method (like orthogonal regression etc.) which is beyond the scope of this thesis, we just presented peak positions.

Furthermore, as we know the position of the first peak depends on the total density parameter Ω_0 according to the equation (4.14). In case of our fit, the $\Omega_0 \simeq 1.006 \simeq 1$. This means that we live in the universe which is nearly flat (has approximately zero curvature).

¹ A numerical computing environment and programming language developed by MathWorks. MATLAB name is derived from MATrix LABoratory.

Conclusion

This bachelor thesis dealt with the CMB anisotropies. The results presented in previous chapter are the individual graphs of the cross-power spectra evaluated from two anisotropy maps from different DA. At the graphs we can clearly see the first acoustic peak at $l \approx 220$, and the suggestion of the second one. This fact is due to the insufficient resolution and uncertainties of window function and exclusion mask which caused our spectra to be noised. Below is a comparison of our (fitted) unbinned data with the official WMAP 7-year results available through LAMBDA. We can see that our results match the WMAP results at the smaller multipoles, but on the higher multipoles they slightly deviate.

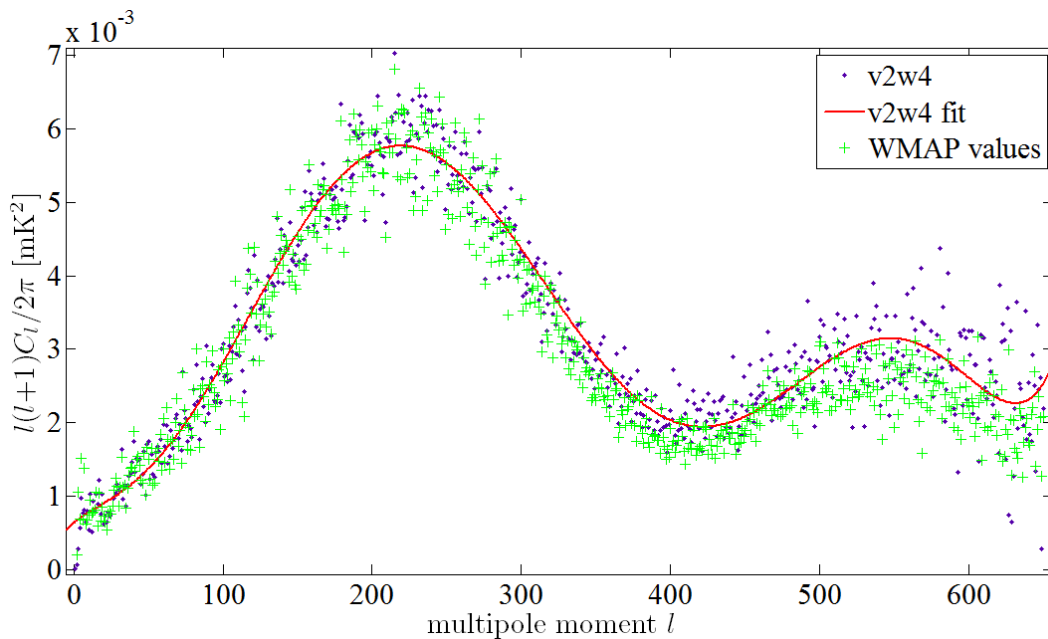


Figure 5.12: The comparison of WMAP data and our results.

The fitting of the cross-power spectrum evaluated from maps V2 and W4 also showed that the first peak is at $l \approx 220$, which implies that our universe is nearly flat. Furthermore, we can see even second acoustic peak at the $l \approx 547$, but due to the relative large deviations of data points from the fitting curve, this result yields also a large error. The positions of the peaks presented in Page et. al (2003)[53] are $l = 220.1 \pm 0.8$ for the first acoustic peak and $l = 546 \pm 10$ for the second one, which is a very good agreement with our results.

List of References

- [1] Scott, Douglas and White, Martin. Cosmic Microwave Background – Introduction [online]. Last revision on 10th of February 2000 [cit. 2011-10-27]. Available from: http://www.astro.ubc.ca/people/scott/cmb_intro.html.
- [2] Sean Carroll. Nobel Prize to Mather and Smoot for CMB Anisotropies [online]. [cit. 2012-05-05]. Available from: <http://blogs.discovermagazine.com/cosmicvariance/2006/10/03/nobel-prize-to-mather-and-smoot-for-cmb-anisotropies/>.
- [3] The CosmicBackground Radiation [online]. [cit. 2011-11-02]. Available from: <http://csep10.phys.utk.edu/astr162/lect/cosmology/cbr.html>.
- [4] LAMBDA – Cosmic Background Explorer [online]. Last revision on 26th of Jun 2008 [cit. 2011-11-13]. Available from: <http://lambda.gsfc.nasa.gov/product/cobe/>.
- [5] Birkinshaw, Mark. The Cosmic Microwave Background Radiation [online]. [cit. 2011-11-10]. Available from: http://ned.ipac.caltech.edu/level5/Birkinshaw/Birk1_1.html.
- [6] Doppler Redshift [online]. [cit. 2011-11-10]. Available from: <http://hyperphysics.phy-astr.gsu.edu/hbase/astro/redshf.html>.
- [7] Jarosik et. al. Seven-Year Wilkinson Microwave Anisotropy Probe (WMAP) Observations: Sky Maps, Systematic Errors, and Basic Results. [cit. 2011-11-10]. Available from: arXiv:1001.4744v1.
- [8] Wright, Edward L. Brief History of the Universe [online]. Last revision on 15th of July 2004 [cit. 2011-12-04]. Available from: <http://www.astro.ucla.edu/~wright/BBhistory.html>.
- [9] Gawiser, Eric and Silk, Joseph. THE COSMIC MICROWAVE BACKGROUND RADIATION [online]. [cit. 2011-12-04]. Available from: <http://ned.ipac.caltech.edu/level5/Sept05/Gawiser2/Gawiser1.html>.
- [10] Big Bang Energy and Time Example [online]. [cit. 2011-12-09]. Available from: <http://hyperphysics.phy-astr.gsu.edu/hbase/astro/bb1c.html>.

- [11] Douglas, Scott. Intermediate FAQs [online]. Last revision on 13th of December 1999 [cit. 2011-12-05]. Available from: http://www.astro.ubc.ca/people/scott/faq_intermediate.html.
- [12] Legendre transformation [online]. [cit. 2012-03-21]. Available from: <http://encyclopedia2.thefreedictionary.com/Legendre+Transformation>.
- [13] Cosmic Microwave Background [online]. [cit. 2012-03-21]. Available from: lambda.gsfc.nasa.gov/product/map/team_pubs/encyclopedia_elw.ps.
- [14] Ostlie, Dale A. and Carroll, Bradley W. An Introduction to Modern Astrophysics. Second Edition. San Francisco: Pearson Education, Inc, c2007. 1358p. ISBN 0-321-44284-9.
- [15] Weisstein, Eric W. Legendre Polynomial [online]. [cit. 2012-04-29]. Available from: <http://mathworld.wolfram.com/LegendrePolynomial.html>.
- [16] Legendre polynomials – orthogonality [online]. [cit. 2012-04-18]. Available from: <http://physicspages.com/2011/03/18/legendre-polynomials-orthogonality>.
- [17] Rocha, Graca. Comparison of Microwave Background. Radiation models and experiments [online]. [cit. 2012-04-18]. Available from: www.mrao.cam.ac.uk/yerac/rocha/rocha.ps.
- [18] Gawiser, Eric and Silk, Joseph. THE COSMIC MICROWAVE BACKGROUND RADIATION [online]. [cit. 2011-11-17]. Available from: <http://ned.ipac.caltech.edu/level5/Sept05/Gawiser2/Gawiser3.html>.
- [19] Hu, Wayne. Seing Sound [online]. [cit. 2011-12-05]. Available from: <http://background.uchicago.edu/~whu/physics/acoustic.html>.
- [20] A. Kogut et. al. Dipole Anisotropy in the COBE-DMR First-Year Sky Maps [online]. [cit. 2011-12-10]. Available from: arXiv:astro-ph/9312056v1.
- [21] A. H. Jaffe et.al. Determining Foreground Contamination in Cosmic Microwave Background Observations: Diffuse Galactic Emission in the MAXIMA-I Field [online]. [cit. 2011-12-10]. Available from: <http://iopscience.iop.org/0004-637X/615/1/55/fulltext/57496.text.html>.
- [22] B. Gold et. al. even-Year Wilkinson Microwave Anisotropy Probe (WMAP) Observations: Galactic Foreground Emission [online]. [cit. 2011-12-10]. Available from: <http://iopscience.iop.org/0004-637X/615/1/55/fulltext/57496.text.html>.
- [23] Penzias, A. A. and Wilson, R. W. A Measurement of Excess Antenna Temperature at 4080 Mc/s.[online]. [cit. 2011-12-14]. Available from SAO/NASA Astrophysics Data System (ADS):1965ApJ...142..419P.

- [24] Richmond, Michael. The Microwave Background [online]. [cit. 2011-12-14]. Available from: <http://spiff.rit.edu/classes/phys240/lectures/cmb/cmb.html>.
- [25] Levinel, Alaina G. The Large Horn Antenna and the Discovery of Cosmic Microwave Background Radiation [online]. [cit. 2011-12-14]. Available from: <http://www.aps.org/programs/outreach/history/historicsites/penziaswilson.cfm>.
- [26] Timeline of cosmic microwave background astronomy [online]. [cit. 2011-12-14]. Available from: http://en.wikipedia.org/wiki/Timeline_of_cosmic_microwave_background_astronomy.
- [27] Critical Density [online]. [cit. 2012-02-20]. Available from: <http://www.astro.virginia.edu/~jh8h/glossary/criticaldensity.htm>.
- [28] Big Bang Cosmology [online]. [cit. 2012-02-20]. Available from: http://map.gsfc.nasa.gov/universe/bb_theory.html.
- [29] Big Bang Cosmology [online]. [cit. 2012-02-21]. Available from: http://map.gsfc.nasa.gov/universe/bb_concepts.html.
- [30] The Big Bang and the Expansion of the Universe [online]. [cit. 2011-02-25]. Available from: <http://www.atlasoftheuniverse.com/bigbang.html>.
- [31] Density parameter [online]. [cit. 2012-03-02]. Available from: <http://hyperphysics.phy-astr.gsu.edu/hbase/astro/denpar.html>.
- [32] Expanding Universe [online]. [cit. 2012-03-08]. Available from: <http://hyperphysics.phy-astr.gsu.edu/hbase/astro/hubble.html>.
- [33] Deceleration Parameter [online]. [cit. 2012-03-012]. Available from: <http://astronomy.swin.edu.au/cms/astro/cosmos/d/Deceleration+Parameter>.
- [34] Deceleration Parameter [online]. [cit. 2012-03-014]. Available from: <http://www.answers.com/topic/deceleration-parameter>.
- [35] WMAP Mission Overview [online]. [cit. 2012-01-02]. Available from: <http://wmap.gsfc.nasa.gov/mission/>.
- [36] WMAP Observatory Overview [online]. [cit. 2012-01-02]. Available from: <http://wmap.gsfc.nasa.gov/mission/observatory.html/>.
- [37] WMAP Timeline [online]. [cit. 2012-01-05]. Available from: <http://wmap.gsfc.nasa.gov/news/events.html/>.
- [38] WMAP Mission Specifications [online]. [cit. 2012-01-05]. Available from: http://wmap.gsfc.nasa.gov/mission/observatory_spec.html.
- [39] WMAP Scan Strategy [online]. [cit. 2012-01-05]. Available from: http://wmap.gsfc.nasa.gov/mission/observatory_scan.html.

- [40] brightness temperature [online]. [cit. 2012-01-05]. Available from: http://www.daviddarling.info/encyclopedia/B/brightness_temperature.html.
- [41] brightness temperature [online]. [cit. 2012-01-05]. Available from: <http://scienceworld.wolfram.com/physics/BrightnessTemperature.html>.
- [42] Sky Maps [online]. [cit. 2012-04-04]. Available from: http://lambda.gsfc.nasa.gov/product/map/dr4/skymap_info.cfm.
- [43] WMAP Data Products [online]. [cit. 2012-04-04]. Available from: http://lambda.gsfc.nasa.gov/product/map/current/m_products.cfm.
- [44] The WMAP Science Working Group. Wilkinson Microwave Anisotropy Probe (WMAP) Seven-Year Explanatory Supplement [online]. [cit. 2012-04-03]. Available from: http://lambda.gsfc.nasa.gov/product/map/current/pub_papers/sevenyear/supplement/WMAP_supplement.pdf.
- [45] Intensity and Polarization Exclusion Masks [online]. [cit. 2012-04-04]. Available from: http://lambda.gsfc.nasa.gov/product/map/dr4/masks_info.cfm.
- [46] HEALPix Introduction [online]. [cit. 2012-04-07]. Available from: <http://healpix.jpl.nasa.gov/>.
- [47] Hinshaw etl. al. First Year Wilkinson Microwave Anisotropy Probe (WMAP) Observations: Angular Power Spectrum [online]. [cit. 2012-04-07]. Available from: arXiv:astro-ph/0302217v1.
- [48] Balbi et. al. CMB Power Spectrum Estimation for the Planck Surveyor [online]. [cit. 2012-04-14]. Available from: arXiv:astro-ph/0203159v2.
- [49] Balbi, Amedeo. The Music if the Big Bang: The Cosmic Microwave Background and the New Cosmology. 1st edition, 2008. Berlin: Springer-Verlag, c2008. 158p. ISBN 978-3-642-09749-2.
- [50] Heller, Michael and Woodin, W. Hugh. Infinity: New Research Frontiers. 1st edition, 2011. New York: Cambridge University, c2011. 311p. ISBN 978-1-107-00387-3.
- [51] Observing the CMB [online]. [cit. 2012-05-03]. Available from: http://www.ita.uni-heidelberg.de/~dullemond/lectures/cosmology_2011/Chapter_8.pdf.
- [52] The HEALPix primer [online]. [cit. 2012-05-03]. Available from: <http://healpix.jpl.nasa.gov/pdf/intro.pdf>.
- [53] Page et. al. First-Year Wilkinson Microwave Anisotropy Probe (WMAP) Observations: Interpretation of the TT and TE Angular Power Spectrum Peaks [online]. [cit. 2012-05-05]. Available from: arXiv:astro-ph/0302220v2.

